REPETITIVE CONTROL OF A NOVEL LINEAR MAGNETOSTRICTIVE ACTUATOR

A Thesis

by

RUIKANG ZHU

Submitted to the Office of Graduate and Professional Studies of
Texas A&M University
in partial fulfillment of the requirements for the degree of

MASTER OF SCIENCE

Chair of Committee,	Won-jong Kim
Committee Members,	Bryan P. Rasmussen
	Hamid A. Toliyat
Head of Department,	Andreas Polycarpou

August 2014

Major Subject: Mechanical Engineering

ABSTRACT

This thesis presents the repetitive control (RC) design of a novel linear magnetostrictive actuator. A repetitive controller is developed and tested on a novel linear magnetostrictive actuator to improve the tracking accuracy of the actuator to a periodic signal.

The repetitive controller is designed based on an estimated model of the system which does not consider the model nonlinearities. In the repetitive controller, a learning controller helps the actuator track the reference signal faithfully. A Butterworth low-pass filter is designed to stabilize the system in high frequencies. The parameters of the learning controller and the low-pass filter are initially tuned during simulation and then tested in the experiment. The stability, robustness, convergence rate, and performance are discussed in the RC design. The trade-off between robustness and performance is taken into serious consideration. In the experiment part, sinusoidal and triangular reference signals are used to test the tracking performance of the repetitive controller.

Simulation results show that the maximum tracking error to a sinusoidal signal with a magnitude of 1 mm could be limited to 0.1 μm, which is 0.01% of the reference input. Experiment results demonstrate that the maximum tracking error to a sinusoidal reference signal with a magnitude of 0.5 mm and frequency of 0.1 rad/s could decrease to 20 μm, which is 4% of the reference signal. Compared with the previous result, the maximum tracking error to a sinusoidal reference signal with a magnitude of 0.5 mm decreased from 100 μm to 20 μm. The experimental results demonstrate that the repetitive

controller works effectively to improve the tracking accuracy of the linear magnetostrictive actuator.

ACKNOWLEDGMENTS

First and foremost, I would like to express my sincere gratitude to my advisor, Professor Won-jong Kim, for being a teacher and a mentor who provides great support, encouragement, and understanding during my master's study. He is always willing to help me with his thoughtful ideas and profound knowledge, and encourages me when I am depressed with problems in my research. He has obviously influenced my life considerably.

I would like to thank Professor Hamid A. Toliyat for serving as my committee member. I especially thank Professor Bryan Rasmussen for serving as my committee member, and his meaningful suggestions in my research. I much enjoyed taking his control system design course and learned a lot about control system theory from it.

I would like to thank all my past and present lab mates in Precision Mechatronics Laboratory. They are always willing to help me when I have a problem. I have a great time studying and researching with them.

My special thanks go to Chien-Fan Chen. He helped me understand the working principle and operation procedures of the novel linear magnetostrictive actuator.

I would like to thank my parents, for their unconditional love, support, and faith in me. I am grateful to them for providing such a great opportunity to me to study in the USA and encouraging me during my entire study.

Finally, I would like to thank all the family members, friends, and those who helped and supported me in my life.

TABLE OF CONTENTS

Page

LIST OF FIGURES

Page

CHAPTER I

INTRODUCTION

1.1 History and Application of Magnetostrictive Actuators

1.1.1 Linear Actuators

Linear actuators have been widely employed in machine tools and industrial machinery where linear motion is required. Being different from the traditional electric motors that create rotational motion, linear actuators generate motion in a straight trajectory. However, conventional linear actuators have some disadvantages when space and power-consumption limitation is imposed upon. For example, hydraulic actuators that could generate large force are not applicable when there is insufficient space to contain the hydraulic system, while direct-drive linear electric actuators could not generate large force comparing with hydraulic actuators [1]. Hence, linear actuators based on giant-magnetostrictive materials were introduced to overcome the limitations of conventional linear actuators.

1.1.2 Giant-Magnetostrictive Materials

Magnetostriction is the primary working principle of the magnetostrictive actuators. It describes a physical phenomenon of ferromagnetic materials that causes them to change shape when subjected to an external magnetic field. Joule first reported observing change in the length of a rod of nickel in 1842. Fig. 1.1 shows the magnetostrictive curve under a varying external magnetic field, where magnetostriction strain is $\lambda=\Delta L/L$.

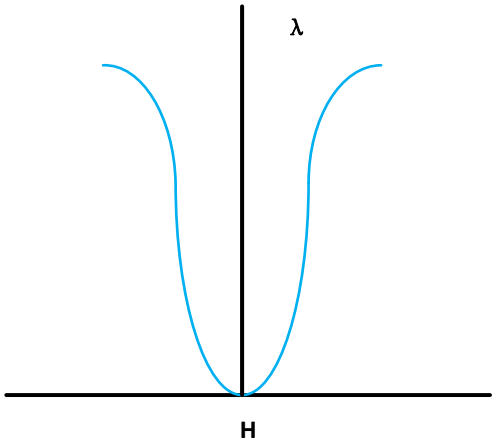

Fig. 1.1. Magnetostriction curve under a varying external magnetic field

Unlike the conventional magnetic actuators that use the Lorentz force to produce physical displacement, magnetostrictive actuators use special materials that can change their shapes when exposed to external magnetic fields [2]. Among these special materials, Terfenol-D, an alloy of formula $Tb_{0.3}Dy_{0.7}Fe_{1.92}$ was firstly developed in the 1950s. The magnetostriction of this material is up to 2000 ppm, which is the highest among all alloy [3] [4]. Since the magnetostrictive actuator has small magnetostriction strain level, it could generate high force within a small range of actuation [1].

1.1.3 Magnetostrictive Actuators with Direct and Indirect Motion Control

Magnetostrictive actuators could be classified into two types according to different motion styles: direct motion control and indirect motion control [5]. In magnetostrictive actuators with direct motion control, one side of the magnetostrictive material is fixed.

The material elongates when exposed to external magnetic fields. The disadvantage of this type of design is limited range of motion. In magnetostrictive actuators with indirect motion control, however, neither side of the magnetostrictive material is fixed so that the actuators can generate motion in two directions. They can provide a wider range of motion with a larger force capacity than the magnetostrictive actuators with direct motion control.

In 1988, Kiesewetter [6] designed a special magnetostrictive motor by putting a Terfenol-D rod inside a tight-fitting tube [7]. Both the longitudinal and radial strains are used in the Terfenol-D rod. The rod can move inside the tube with a peristaltic motion. The main drawback of this design is that the contact between the tube and Terfenol-D rod may lead to the wear of the material situation. The force-generation capacity of the motor will decrease after prolonged usages.

1.1.4 Extended-Range Linear Magnetostrictive Motor

Kim, et al. designed an extended-range linear magnetostrictive motor with double-sided three-phase stators to overcome the shortcomings of the Kiesewetter motor. They placed a laminated Terfenol-D slab between two spring loaded plates to ensure the proper contact regardless of thermal expansion, wear, or motion [8]. However, the power consumption of the actuator is relatively high due to the eddy-current losses. Fig. 1.2 shows the photograph of the extended-range linear magnetostrictive actuator with double-sided stators [8].

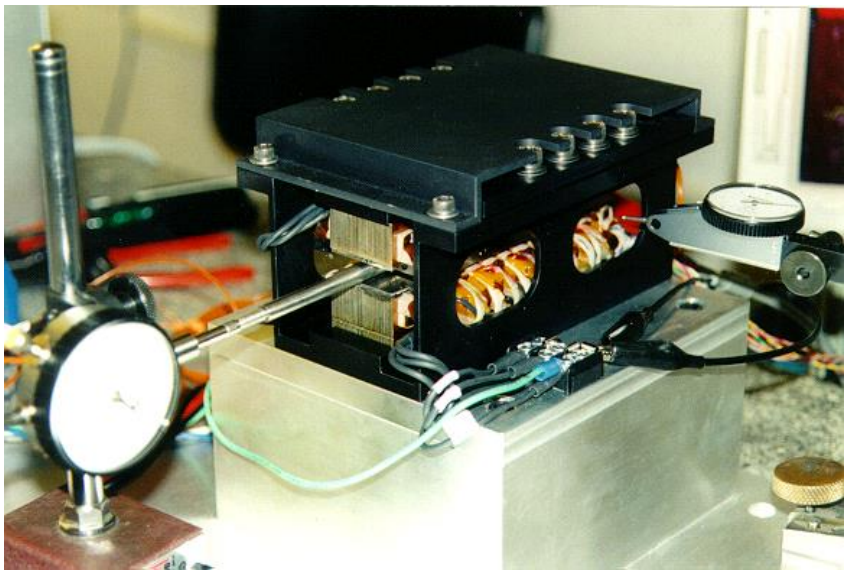

Fig. 1.2. Photograph of the extended-range linear magnetostrictive actuator with double-sided stators [8]

1.1.5 Novel Low-Power Linear Magnetostrictive Actuator

Kim and Sadighi developed a novel low-power linear magnetostrictive actuator to reduce the power consumption a local excitation approach [1]. A new structure for coils is developed to produce higher magnetostrictive strain. This special design allows for either conventional or local multiphase excitation to be implemented on the actuator. Fig. 1.3 shows the photograph of the low-power linear magnetostrictive actuator. This actuator is used to verify the working of the repetitive controller in this thesis.

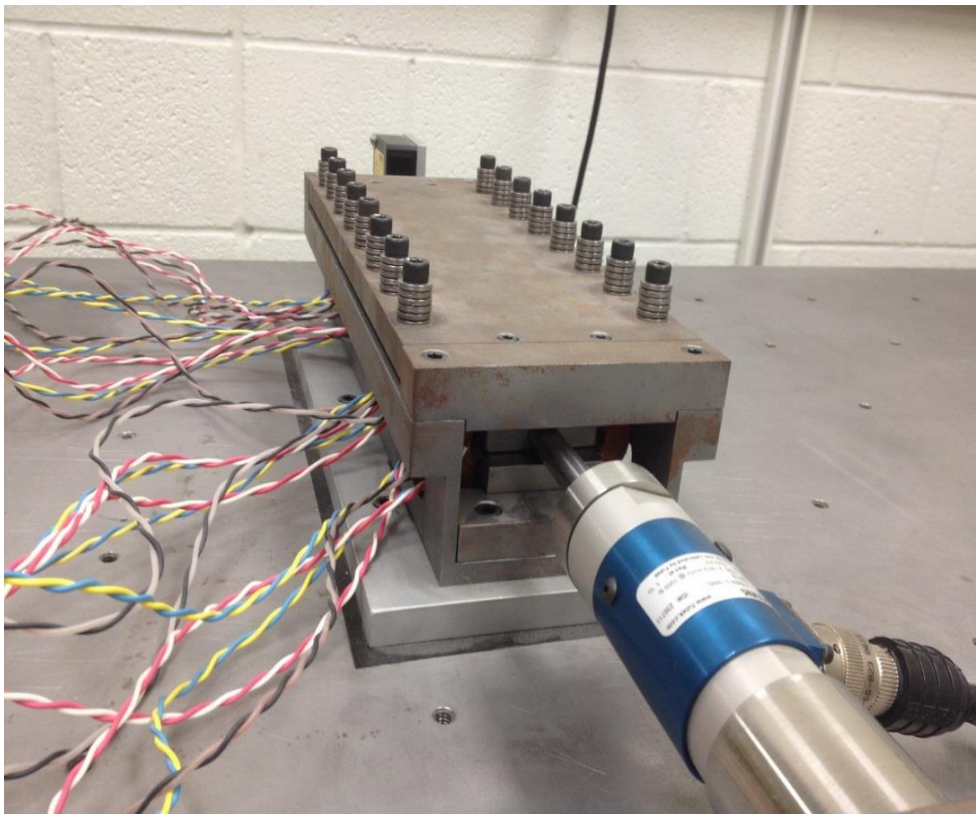

Fig. 1.3. Photograph of the low-power linear magnetostrictive actuator

1.1.6 Application of Magnetostrictive Actuators

Magnetostrictive actuators have been widely applied in various applications due to the advantages of high precision, wide bandwidth, and good reliability. A typical application is active vibration control. Actuators used for active vibration control should be accurate, and have a large range of actuation. Magnetostrictive actuators can have a better accuracy than the actuators with traditional transducer materials. Furthermore, the magnetostriction of Terfenol-D does not decay over time or after numerous cycles of operation, which is proved to be suitable for vibration control [9]. Magnetostrictive Actuators are also applied in manufacturing and damage detection due to the advantages

of larger force capacity [10] [11].

1.2 Repetitive Control Methods

Many signals are periodic in engineering applications. Some signals may not be strictly periodic, but can be approximately regarded to be periodic in a large time scale. Such signals exist in electrical generators and motors, engines, convertors, etc. [12]. Thus, it is necessary to devise a method to track a periodic signal or to reject a periodic disturbance in the system. Repetitive control (RC) was developed to solve these problems. RC was firstly introduced by Inoue, et al. in 1981 and widely used to reject periodic disturbances or track reference signals [13] [14].

The internal-model principle (IMP) is the theoretical foundation of RC. This method was first proposed by Francis and Wonham [15]. They introduced a brand-new idea to incorporate the representation of the process in order to track reference signals or reject disturbances. Based on IMP, the control system collects information from previous periods to modify the control signal in the current period so that the system could "learn" to reject disturbances or track periodic reference signals after several trials [12]. More specifically, this signal is treated as the output of an autonomous generator in the control system.

RC is a special type of an IMP controller. Any controller containing a periodic signal generator is regarded as a repetitive controller. Fig. 1.4 shows such a periodic signal generator. A component with a specific time delay and an appropriate initial function is applied to generate any desired periodic signal [16].

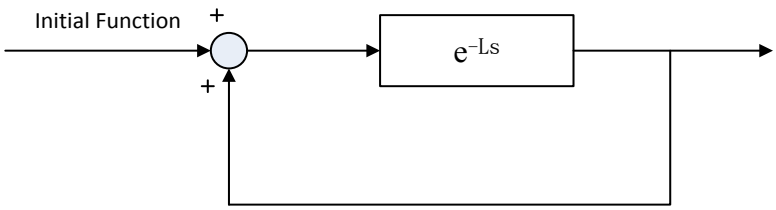

Fig. 1.4. Block diagram of periodic signal generator

Inoue, et al. used a continuous-time model when they developed RC [13] [14]. However, continuous-time RC has difficulty in compensating for all high-frequency components in periodic reference inputs or disturbances due to the fact that the system stability is hard to be guaranteed [17][18]. Thus the digital implementation of RC was discussed by several researchers to address this difficulty. The first approximate digital implementation of repetitive controllers was introduced by Nakano and Hara [19]. Tomizuka, et al. firstly introduced the discrete formulation of RC with discrete-time analysis and synthesis [20]. Compared with a continuous-time model, the structure of digital implementation is simpler. Figs. 1.5 and 1.6 show a simplified and general form of the discrete-time RC model.

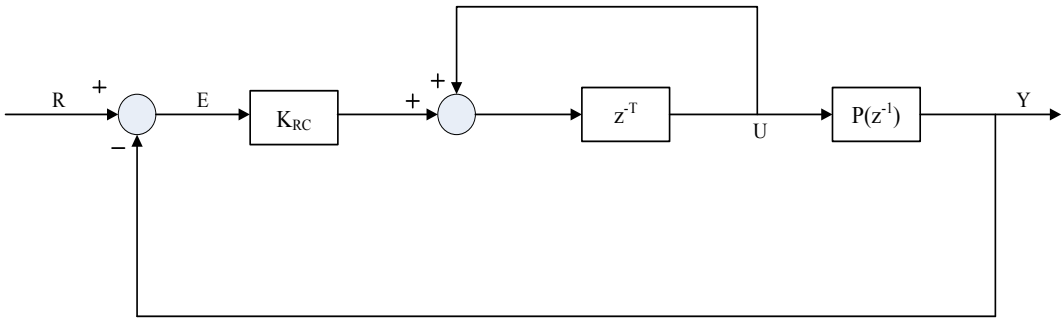

Fig. 1.5. Block diagram of a simplified form of the discrete-time RC model

The major difference between the general structure and the simplified one is that the general structure contains two filters: the learning controller L (L_{RC}) and the low-pass filter (LPF) Q (Q_{RC}).These two filters are implemented to guarantee the stability of the RC and optimize its performance.

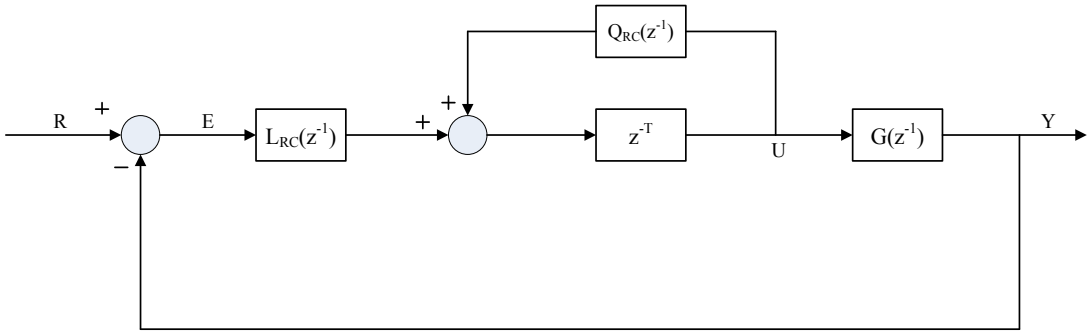

Fig. 1.6. Block diagram of a general form of the discrete-time RC model

RC has been widely applied in various engineering applications. Its representative applications include the suppression of vibration studied by Hillerstrom, et al. [21] [22], controller design of hard-disk drives by Kempf, et al. [23], robot control under periodic commands by Cosner, et al. [24].

1.3 Overview of the Thesis

This thesis contains five chapters. Chapter I presents a literature review and a history of magnetostrictive actuators, and an introduction of RC methods.

Chapter II discusses the working principle and the electromagnetic design of the linear magnetostrictive actuator. In this chapter, the general structure and specific components of the mechatronic system are introduced.

Chapter III presents a detailed RC design approach. In this chapter, the design methodology of RC, including the learning controller L, the LPF Q, and the implementation of RC with and without the Q-filter are discussed.

Chapter IV gives the simulation and experimental results with RC. Results analyses and comparison with previous work are presented in this chapter.

Chapter V concludes this thesis with a summary of my achievements and suggestions for future work. Appendices include the MATLAB code used to design the RC and the Simulink block diagrams used to control the magnetostrictive actuator.

1.4 Contributions

The main contribution of this thesis is the design and implementation of the RC in the magnetostrictive actuator. This RC is able to reduce the tracking error to a periodic signal after several periods. Simulation and experimental results, and comparisons with previous work are presented in the thesis.

Simulation results show that the maximum tracking error to a sinusoidal signal with a magnitude of 1 mm could be limited to 0.1 μm, which is 0.01% of the reference input. Experiment results demonstrate that the maximum tracking error to a sinusoidal reference signal with a magnitude of 0.5 mm and frequency of 0.1 rad/s could decrease to 20 μm, which is 4% of the reference signal. Compared with the previous result, the maximum tracking error to a sinusoidal reference signal with a magnitude of 0.5 mm decreased from 100 μm to 20 μm.

CHAPTER II

ELECTROMAGNETIC DESIGN

This chapter discusses the working principle and the electromagnetic design of the linear magnetostrictive actuator. Sections 2.1 and 2.2 describe the working principle and the empirical model of the linear magnetostrictive actuator. Sections 2.3 and 2.4 discuss the magnetic design and the winding design. Sections 2.5 to 2.7 give the working principle and the description of the mechatronic system.

2.1 Working Principle

The working principle of the linear magnetostrictive actuator is shown in Fig. 2.1. The general design idea is to create a peristaltic motion of the Terfenol-D slab that is kept under pressure by generating a traveling magnetic field [1].

The Terfenol-D slab is kept in a tight fit between two stators. The stators are designed to enhance the magnetic flux density inside the active element. Twenty-four coils surround the Terfenol-D slab to generate the travelling magnetic field. The slab changes its shape along the magnetic field lines when interacted with the magnetic field. The slab stretches while its cross-section area decreases since its total volume remains the same. The stretch releases the slab from the tight fit with the stators. When the magnetic field travels to the neighboring portion of the slab, it contracts to its original shape and locks itself between the stators while the neighboring portion stretches. The entire Terfenol-D slab moves to the opposite of the direction of the magnetic field when the magnetic field

travels through the slab. A peristaltic motion of the slab is created by repeating the same processes.

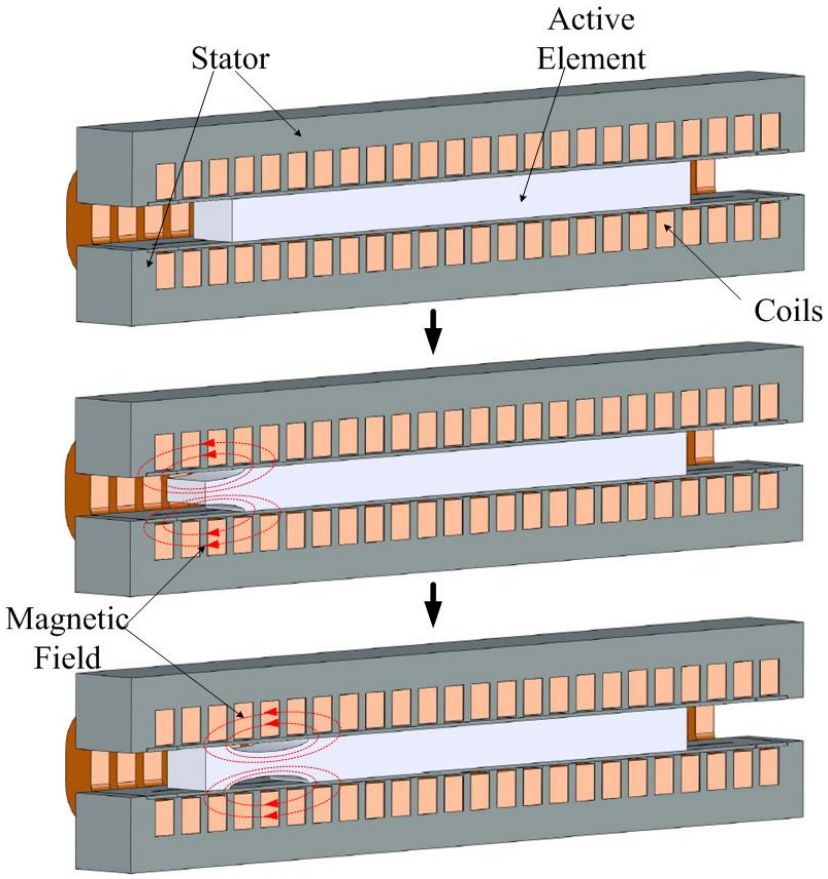

Fig. 2.1. Working Principle of the Linear Magnetostrictive Actuator [25]

2.2 Empirical Model

Experimental results show that the speed of this magnetostrictive actuator is a function of switching frequency, peak magnetostrictive strain, and external load [8]. With the magnetostrictive actuator under a local multi-phase operation, the empirical model of

this actuator is given as follows [8]:

$$v = Nfp(\varepsilon_{\max} - \frac{F}{EA_T}) \qquad (2.1)$$

where

N number of phases (3)

f local multiphase excitation frequency (Hz)

p slot pitch (10.9 mm)

ε_{max} peak magnetostrictive strain under no-load condition

F external load (N)

E Young's modulus of Terfenol-D (35 GPa)

A_T cross-sectional area of the Terfenol-D slab (400 mm^2)

2.3 Finite-Element Analysis in Magnetic Design

A finite-element analysis (FEA) approach was used in the previous research to analyze the impact of the thickness of Tefernol-D material on the magnetic flux density [25]. The main purpose of this analysis is to enhance the magnetic flux density inside the active element. The benefit of a high magnetic flux density can be seen from (2.1) that if the magnetic flux density increases, the power requirement decreases while the force capacity increases. The FEA results show the magnetic flux density is higher with a thinner active element [25]. However, the thickness of the active element is limited by the space between the stators of the magnetostrictive actuator. Therefore, a minimum required space for the force transmission assembly needs to be considered during the magnetic design.

Therefore, the thickness of the active element is designed as 12.7 mm to ensure the clearance between the stators and the force transmission assembly since the thickness of force transmission assembly is 11 mm. Finally, 12.7 mm×31.5 mm×200 mm was selected as the dimension of the active element.

2.4 Winding Design

The main purpose of the winding structure design is to generate a 0.6-T magnetic flux density inside the Terfenol-D slab according to the FEA [25]. To achieve this design goal, the actuator incorporates 24 coils, and each coil includes 273 turns of AWG ＃24 wire. The required tools were manufactured and the coils were wound by Wire Winders. The dimension of the coils is shown in Fig. 2.2 [25].

The length of wire in each coil is approximately 47.5 m, which has a resistance of 4 Ω, according to the American wire gauge (AWG) standard. The exact resistance and inductance of each wire measured by an RCL meter is 4.28 Ω and 9.7 mH, respectively.

2.5 Power Electronics

The local three-phase excitation method was developed and implemented in the previous research [25]. The purpose of the power electronics is to direct the current through three adjacent coils and move to the other side of the coils as shown in Fig. 2.3.

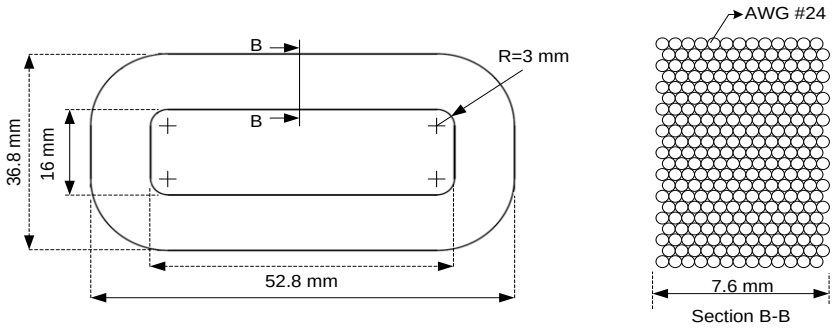

Fig. 2.2. Wire arrangement in the coils [25]

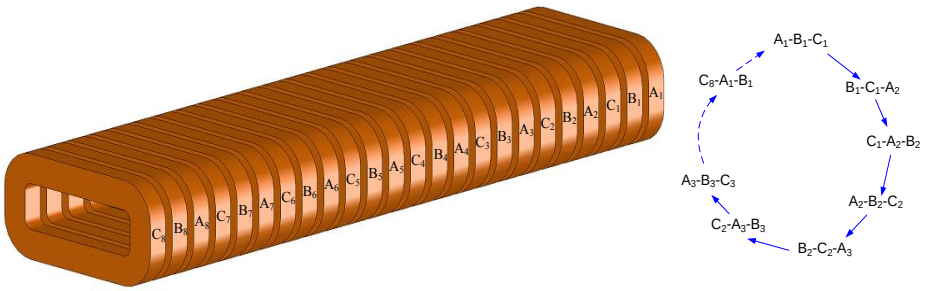

Fig. 2.3. Coil arrangement and the local three-phase excitation sequence [25]

2.5.1 Power MOSFET

A metal-oxide-semiconductor field-effect transistor **(**MOSFET) is used for switching electronic signals. It is a three-terminal device with a drain (D), source (S), and gate (G). As illustrated in Fig. 2.4, the n- channel MOSFET has a p-type substrate, an n-type source and drain, and a silicon dioxide layer. When a positive DC voltage is applied to the gate, a conducting channel is created in the substrate which contains electrons. This is referred to as an n-channel in the p-type substrate [26].

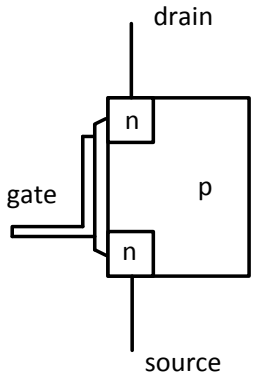

Fig. 2.4. n-channel enhancement-mode MOSFET

The working principle of the n-channel enhancement-mode MOSFET is described as follows. As shown in Fig. 2.5, if V_{gs} (gate voltage) < V_t (threshold voltage, typically of 2 V), $V_{ds} = 0$, the MOSFET is in the cutoff region and acts as a very large resistor. If $V_{gs} > V_t$, the MOSFET is in the active region (or ohmic region) and acts as a variable resistor controlled by V_{gs}. If V_{gs} grows very large, the MOSFET is in saturation and the current I_{ds} remains constant [26]. The characteristic curves of the n-channel enhancement-mode MOSFET are shown in Fig. 2.6.

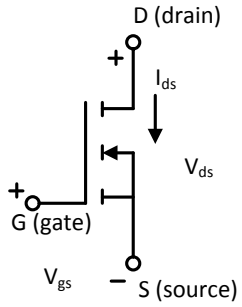

Fig. 2.5. Schematic symbol of an n-channel enhancement-mode MOSFET

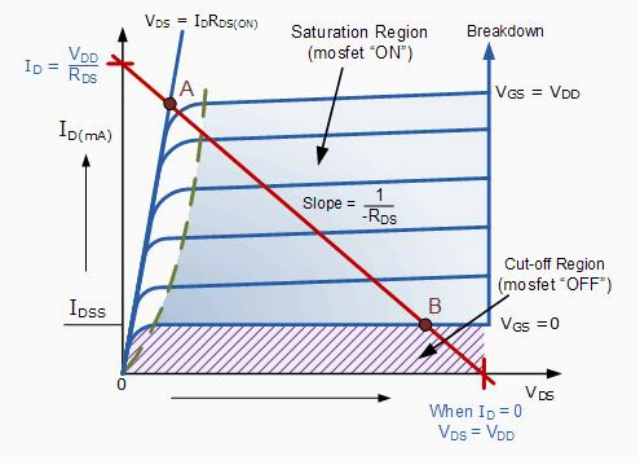

Fig. 2.6. n-channel enhancement-mode MOSFET characteristic curves [27]

2.5.2 Switching Boards

Three switching boards were designed to direct the current into three adjacent coils and switch to the other side of the coil [25]. Model E3644A by Agilent was selected as the power supply to supply power for each board. Each switching board includes eight power MOSFETs, eight MOSFET drivers, eight flyback diodes, three inverters, and one 3-line to 8-line decoder [25]. The switching frequency of the power MOSFETs is controlled by the digital inputs/outputs (I/Os) of a digital-signal-processing (DSP) board. And the specific switching frequency strategy is designed in the Simulink software. The schematic diagram of the digital circuit and power electronics for one phase is shown in Fig. 2.7.

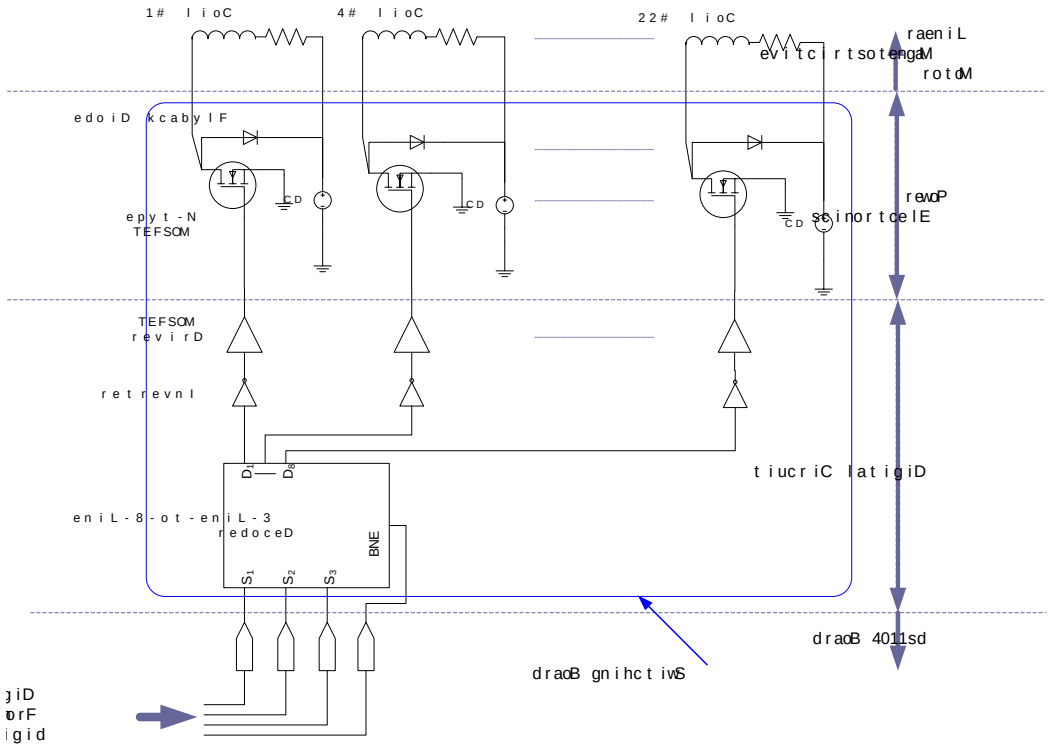

Fig. 2.7. Schematic diagram of digital circuit and power electronics for one phase [25]

2.6 PWM Control

Chen [5] redesigned the switching board based on the previous research. In his control system design, the current needs to be controlled in each coil of the magnetostrictive actuator. Thus the following electronic control is designed to achieve the goal. Pulse-width modulation (PWM) amplifiers have the advantages that they drive bipolar power transistors rapidly between cutoff and saturation or turn FETs on and off. In both cases, power dissipation is small [26]. Therefore, PWM amplifiers are applied to the electric system to control the current lower power consumption. The 3-to-8-line decoder applied in the previous design can send the PWM signal from one of its inputs.

In the RC design, the PWM amplifies is also implemented to control the currents directed to the actuator.

2.7 Mechatronic System

The structure of the mechatronic system is as shown in Fig. 2.8. A PC is interfaced with a DSP board to control the entire system. The position of the active element is measured by a laser distance sensor and the current of the coils in the magnetostrictive actuator is measured by the current transducers. These signals are directed by the A/D channels of the DSP and could be stored on the PC. In order to control the phase current, the PWM signal is directed from the slave I/O PWM connector of the DSP board to the 3-to-8-line decoder.

2.7.1 DS1104 R&D Controller Board

The DS1104 R&D controller board shown in Fig. 2.9 is a single-board system with real-time interface (RTI) and a set of I/O channels. Specifically, it contains a 32-bit 250-MHz floating-point DSP, with eight analog-to-digital (A/D) channels, eight digital-to-analog (D/A) channels, twenty digital I/O channels. The advantage of the DS1104 board is that the RTI uses a Simulink block diagram to configure the I/Os graphically. After the design of the Simulink block diagram is finished, the model code is generated by Real-Time Workshop (or Simulink Coder) and then downloaded to the DSP board. In this way, the implementation time could be minimized [28].

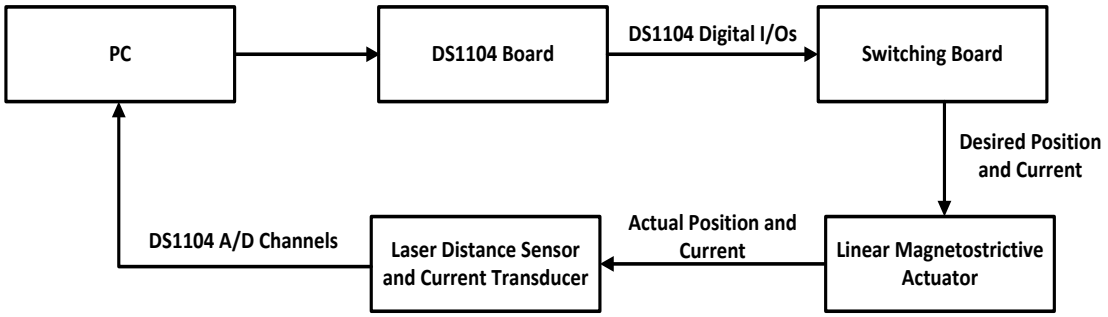

Fig. 2.8. Schematic diagram of the mechatronic system

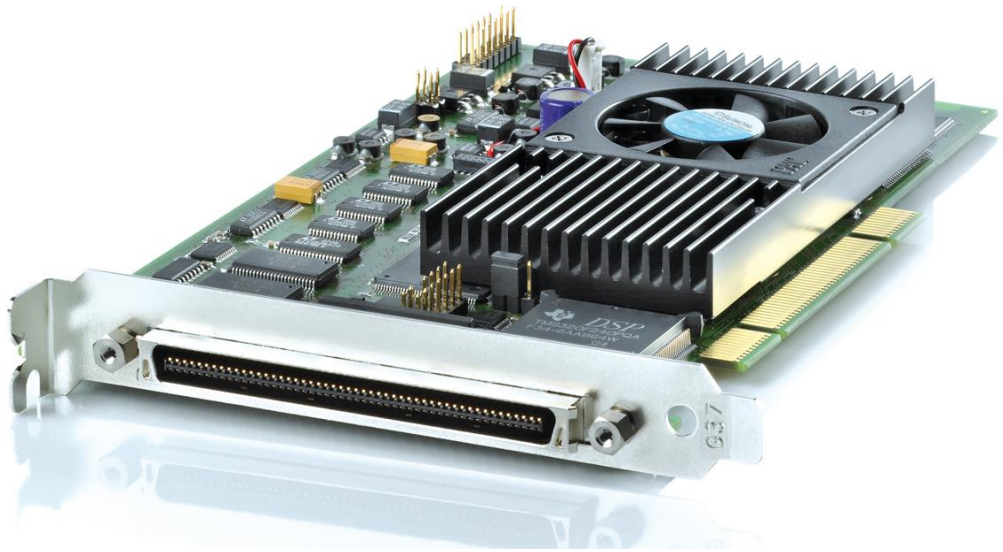

Fig. 2.9. DS1104 R&D controller board [28]

2.7.2 Laser Distance Sensor

The laser distance sensor (model OADM 20I6460/S14F by Baumer Electric) shown in Fig. 2.10 is applied to measure the position of the actuator. The measuring distance range is from 30 mm to 130 mm and the resolution is 5 μm. The output voltage that varies between 0 and 10 VDC is sent to the A/D channels of the DSP board to calculate

the real-time position and displayed in the user interface control panel as shown in Fig. 2.11.

2.7.3 Current Transducer

In the current-control loop, current transducers are required to measure the currents

Fig. 2.10. Laser distance sensor [29]

in the coils. The current transducers implemented in the thesis is (model LA 03-PBA47114) [5]. It has a sensing range of ±4.5 A. The output voltage is within ±4 V, which is sent to the A/D channels of the DSP board and then displayed on the PC.

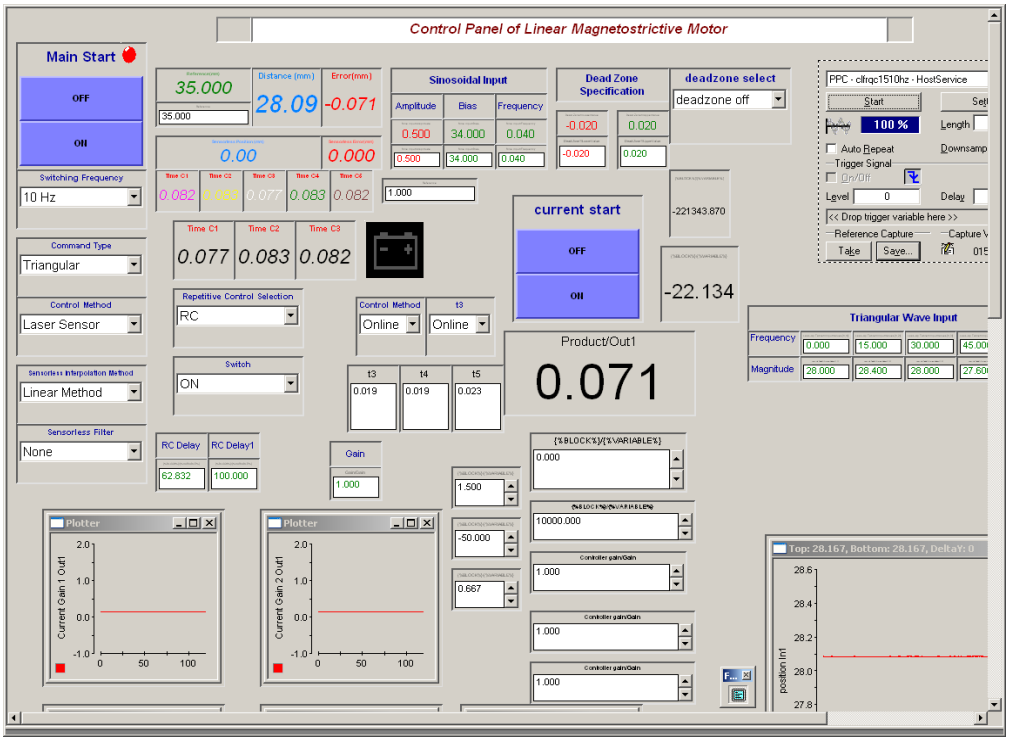

Fig. 2.11. User interface control panel

CHAPTER III

REPETITIVE CONTROL SYSTEM DESIGN

In section 1.2 was introduced the history and principle of RC theory. A detailed controller design approach is described in this chapter. Section 3.1 explains the unsatisfactory actuator performance when existing controllers are applied to the actuator. Next, Section 3.2 gives the design methodology of RC, including the learning controller L and the LPF Q. Section 3.3 discusses the implementation of RC with and without the Q-filter.

3.1 Problem Description

Previous researchers, Kim, Sadighi, and Chen developed several controllers in the linear magnetostrictive actuator system. Kim and Sadighi introduced the first bang-bang controller to the actuator system [1] [2]. A bang-bang controller, also known as a relay controller, was applied to avoid self-oscillations in the system response. Chen designed several types of controller to improve the position precision of the actuator, such as PID controllers tuned by a relay auto-tuning method, sliding-mode controller and linear variable-velocity controller. The PID controller turned out to have the best tracking accuracy among those controllers according to Chen's comparison analysis [5]. Fig. 3.1 shows a closed-loop response to a sinusoidal reference input with an amplitude of 0.5 mm and frequency of 0.04 rad/s tuned by the relay auto-tuning method.

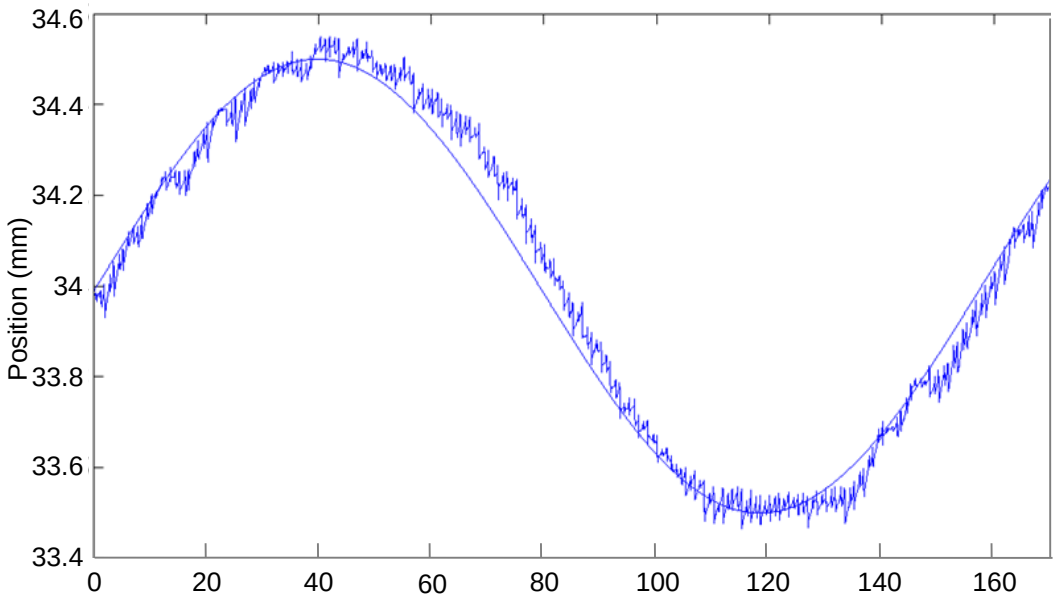

Fig. 3.1. Closed-loop response to a sinusoidal reference input with an amplitude of 0.5 mm and frequency of 0.04 rad/s tuned by relay auto-tuning method [5]

The existing PID controller applied in the closed-loop system improved the actuator performance by reducing the tracking error. However, the tracking error which is over 100 μm is still large comparing with the reference signal with a magnitude of 0.5 mm. Besides, the position trajectory was not as smooth as the input signal. Reverse movement existing in each step of the peristaltic motion. This phenomenon should not take place in such an operation with the consideration of the working principle of the magnetostrictive actuator.

This type of unsatisfactory tracking performances motivated researchers to modify the closed-loop system. That is why repetitive control was introduced to the linear magnetostrictive actuator system to improve the tracking precision.

3.2 Design Methodology

The previous chapter introduced the principle and development of the RC theory, which originated from the IMP. A control system implemented with a repetitive controller is able to track a periodic reference signals or reject disturbances with a known fixed period. In this section, a detailed control design methodology will be presented. Stability, convergence transients, system performance and robustness are the four important criteria of a RC system design [30], which will be discussed in the design.

3.2.1 Periodic Signal Generator

As mentioned in section 1.2, IMP describes an idea to incorporate a part of the representation of the process in order to track reference signals or reject disturbances. One can generate an internal model using a time-delay component with a positive feedback loop. Such a structure is regarded as a periodic signal generator. The continuous-time delay component e^{-Ls} is hard to implement in simulation. In fact, RC is mostly achieved by a discrete-time model. Fig. 3.2 shows the block diagrams of a continuous-time and discrete-time periodic signal generator.

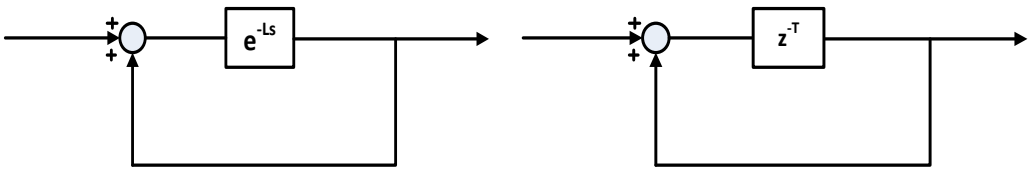

Fig. 3.2. Block diagrams (a) a continuous-time periodic signal generator and (b) a discrete-time periodic signal generator

The representation of a discrete-time internal model of a repetitive controller is shown in (3.1), where T represents the period of the reference input.

$$G(z) = \frac{z^{-T}}{1 - z^{-T}} \tag{3.1}$$

$$G(j\omega) = \frac{e^{-j\omega T}}{1 - e^{-j\omega T}} \tag{3.2}$$

As can be seen in Fig. 3.3, the output generates a continuous sinusoidal signal with one period delay if the input is given by one single period of sinusoidal signal. The delay time is one period of the sinusoidal reference input which is 1 s in this case.

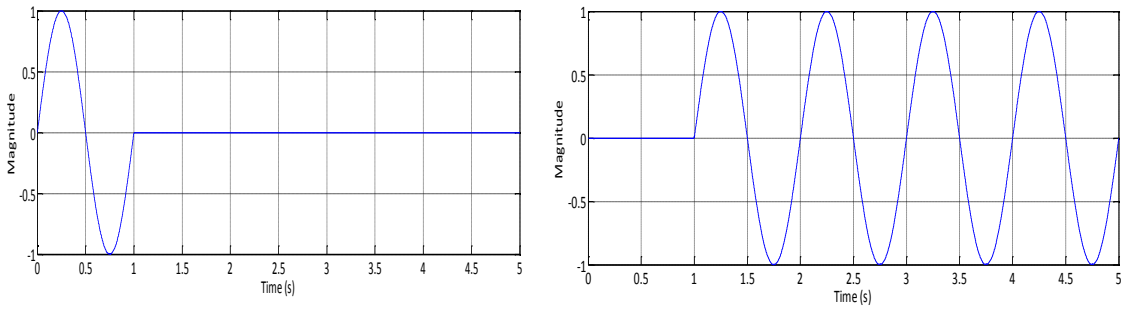

Fig. 3.3. Time response of a periodic signal generator

The frequency response of the continuous-time periodic signal generator is given in Fig. 3.4. When $\omega = \frac{2\pi n}{T}, n = 0,1,2,3\ldots$, the magnitude of $G(j\omega) = \frac{e^{-j\omega T}}{1 - e^{-j\omega T}}$ goes to the infinity.

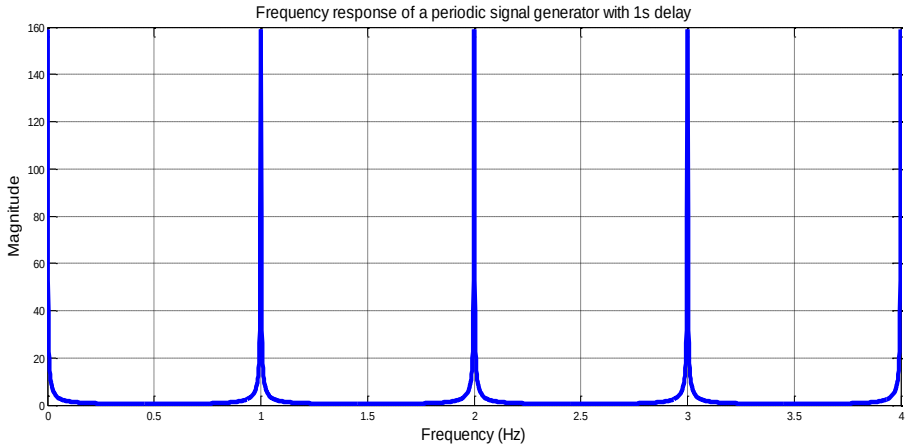

Fig. 3.4. Frequency response of a periodic signal generator with a 1-s delay

3.2.2 Learning Controller Design

A learning controller is designed for the given plant, which determines the performance of the repetitive controller. An appropriate design of the learning controller could help the internal model track the periodic input accurately. Fig. 3.5 shows the basic model of a repetitive controller. Techniques to design the learning controller $L(z^{-1})$ are given as follows.

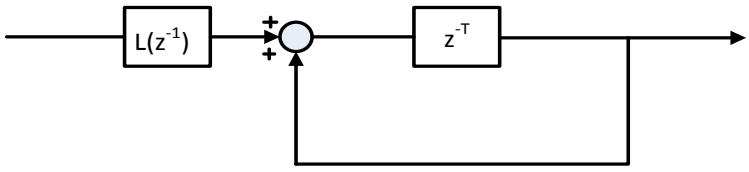

Fig. 3.5. Basic model of a repetitive controller

Fig. 3.6 shows a model of a RC system. The closed-loop transfer function and the

sensitivity function of the model is given as follows.

$$G(z^{-1}) = \frac{z^{-T} L(z^{-1}) C(z^{-1}) P(z^{-1})}{1 - z^{-T}\left(1 - L(z^{-1}) C(z^{-1}) P(z^{-1})\right)} \tag{3.3}$$

$$S(z^{-1}) = \frac{E(z^{-1})}{D(z^{-1})} = \frac{-1}{1 + C(z^{-1}) P(z^{-1})\left(1 + L(z^{-1}) \dfrac{z^{-T}}{1 - z^{-T}}\right)} \tag{3.4}$$

where $D(z^{-1})$ is the disturbance signal and $E(z^{-1})$ is the error signal.

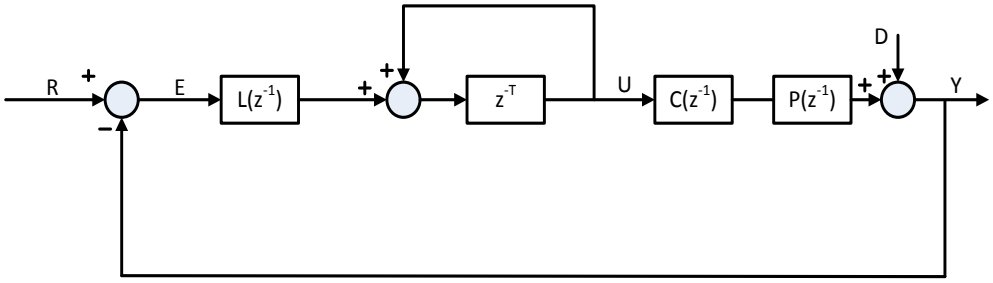

Fig. 3.6. Model of a repetitive control system

When $\omega = \dfrac{2\pi n}{T}, k = 0,1,2,3...$, the magnitude of $G(j\omega) = \dfrac{e^{-j\omega T}}{1 - e^{-j\omega T}}$ goes to infinity, thus $S(z^{-1})$ goes to zero. It indicates that the disturbances will be rejected at those frequencies.

Stability is a key issue when designing any types of controllers. Stability of a RC system is given by the stability of the closed-loop system. In order to check the stability of the system, we can derive that

$$S(z^{-1}) = \frac{-(1 - z^{-T})}{1 + C(z^{-1}) P(z^{-1})} \cdot \frac{1}{1 - z^{-T}\left(1 - L(z^{-1}) G_{CL}(z^{-1})\right)} \tag{3.5}$$

where

$$G_{CL}(z^{-1}) = \frac{C(z^{-1})P(z^{-1})}{1 + C(z^{-1})P(z^{-1})} \tag{3.6}$$

Equation (3.5) can also be represented in the block diagram shown in Fig. 3.7.

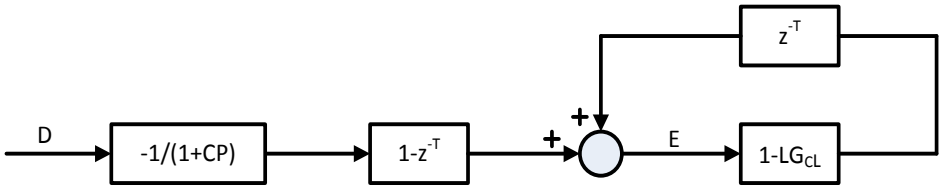

Fig. 3.7. Small gain theorem

A sufficient condition to guarantee the stability is that the gain of the feedback loop is smaller than 1 by the small-gain theorem. The small-gain theorem is describes as follows [31].

Consider a system with a stable loop transfer function $L(jw)$. Then the closed-loop system is stable if

$$\|L(jw)\| < 1 \quad \forall \omega \tag{3.7}$$

where $\|L\|$ denotes any matrix norm satisfying $\|AB\| \le \|A\| \cdot \|B\|$

Therefore, the stability condition for the repetitive control model is given by

$$\left\|1 - L(z^{-1})G_{CL}(z^{-1})\right\| < 1 \tag{3.8}$$

Note that if there is no learning controller in the RC system, the stability condition will become to

$$\left\|1 - G_{CL}(z^{-1})\right\| < 1 \tag{3.9}$$

However, this condition is not always satisfied, which indicates the necessity of the learning controller $L(z^{-1})$. In some papers, the learning controller $L(z^{-1})$ is also called a stabilizing controller.

Tomizuka, et al introduced an inversion method to design the learning controller [32]. For a stable, invertible plant, the compensator could be given by

$$L(z^{-1}) = G_{CL}{}^{-1}(z^{-1}) \tag{3.10}$$

Two issues need to be considered if the compensator is designed with this method. First, if the plant $G_{CL}(z^{-1})$ has zeros outside the unit circle, then $L(z^{-1}) = G_{CL}{}^{-1}(z^{-1})$ has poles outside the unit circle which will make the system unstable. Besides, (3.7) cannot be satisfied in all frequencies especially at high frequencies unless we can derive an accurate plant model. Zero-phase-error tracking control (ZPETC) is one method developed by Tomizuka, et al to design the learning controller to solve the problem [32].

Consider a discrete-time, single-input, single-output (SISO) representation of the closed-loop system that includes the plant and feedback controller,

$$G_{CL}(z^{-1}) = z^{-T}\frac{B(z^{-1})}{A(z^{-1})} \tag{3.11}$$

where z^{-T} indicates that the closed-loop system has T steps delay. Assume $G_{CL}(z^{-1})$ is an asymptotically stable system, thus the all poles of $G_{CL}(z^{-1})$ are located inside the unit circle. The model of the closed-loop system with a learning controller is shown in Fig. 3.8, where $Y_d(k+T)$ is T steps ahead desired output, and $Y(k)$ is the real output.

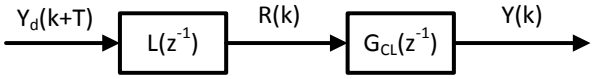

Fig. 3.8. The model of the closed-loop system with a perfect tracking controller

For perfect tracking, we would like to get $Y(k)=Y_d(k)$ .We can easily set $L(z^{-1})=\frac{A(z^{-1})}{B(z^{-1})}$ to achieve perfect tracking if all zeros of the closed-loop system are inside the unit circle, otherwise the controller cannot be implemented. Such a controller is called perfect tracking controller (PTC) [32]. However, if any closed-loop zeros are located outside the unit circle, the PTC would not achieve a perfect tracking performance. Oscillation exists in the output of the PTC. ZPETC is designed under such conditions [32].

First factor $B(z^{-1})$ as:

$$B(z^{-1})=B^u(z^{-1})B^a(z^{-1}) \tag{3.12}$$

where $B^a(z^{-1})$ includes the desirable roots which are inside the unit circle, while $B^u(z^{-1})$ includes the roots outside or on the unit circle and the undesirable roots inside the unit circle.

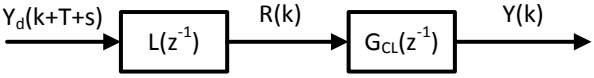

Fig. 3.9. The model of the closed-loop system with a ZPETC

$$L(z^{-1}) = \frac{R(k)}{Y_d(k+T+s)} = \frac{A(z^{-1})B^{u*}(z^{-1})}{B^a(z^{-1})[B^u(1)]^2} \tag{3.13}$$

where

$$B^u(z^{-1}) = b_0 + b_1 z^{-1} + ... + b_s z^{-s} \tag{3.14}$$

$$B^{u*}(z^{-1}) = b_s + b_{s-1} z^{-1} + ... + b_0 z^{-s} \tag{3.15}$$

Note that the input of the controller is T+s steps ahead desired output.

Then combine (3.12), (3.13) and (3.14), the relation from the desired output and the real output is given below.

$$Y(k) = \frac{B^u(z^{-1})B^u(z)}{[B^u(1)]^2} Y_d(k) \tag{3.16}$$

The phase shift brought by this controller is zero at any frequency, and the frequency gain is close to 1 in the low-frequency region.

Another prototype repetitive controller proposed by Tomizuka, et al is given as follows [20]

$$L(z^{-1}) = k_r \frac{z^{-T+d+v} A(z^{-1})\left(z^{-v} B^-(z)\right)}{B^+(z^{-1})b} \tag{3.17}$$

$$b \geq \max_{\omega \in [0,\pi]} \left| B^-(e^{-j\omega}) \right|^2 \tag{3.18}$$

where k_r is the RC gain, v is the order of $B^-(z^{-1})$.

3.2.3 Low-Pass Filter (LPF) Design

The system model is usually inaccurate in high frequencies. Besides, noise exerts a greater influence on the frequency response. Since the model of the plant is uncertain,

one cannot guarantee the performance and the stability of the system in high frequencies. Therefore, it is necessary to introduce a LPF Q to avoid the problem as shown in Fig. 3.10. With this LPF, a small output signal will be sent to the closed-loop plant at high frequencies. Note that with the LPF, the stability condition of the system changes to

$$\left|Q(z^{-1})(1-L(z^{-1})T(z^{-1}))\right|<1 \tag{3.19}$$

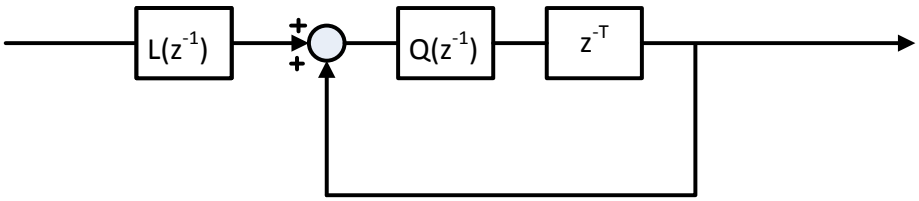

Fig. 3.10. Periodic signal generator with LPF Q

The detailed working principle of the Q filter is shown as follows. At low frequencies, where $\left|Q(z^{-1})\right|\approx 1$, the LPF just filters very little periodic signals in the periodic-signal generator, which indicates the performance will not be affected by the LPF at such frequencies. However, at frequencies higher than the cut-off frequency, where $\left|Q(z^{-1})\right|<1$, the high-frequency component of the periodic signal cannot be captured by the periodic-signal generator. Therefore, the tracking performance will be improved at frequencies higher than the cut-off frequency. On the other hand, according to (3.19), since $\left|Q(z^{-1})\right|$ becomes very small at high frequencies, the problem of the stability at high frequencies is resolved.

There is a trade-off between the system performance and the robustness in such systems regarding the selection of the cut-off frequency. If the cut-off frequency is low, the robustness is better while the tracking performance is compromised at frequencies higher than the cut-off frequency. If the cut-off frequency is high, the tracking performance is good while the stability at higher frequencies cannot be ensured. Filters with different cut-off frequencies will be introduced in the next section. Simulation results in the Chapter IV will illustrate this trade-off.

3.3 Implementation of Repetitive Controller

3.3.1 Simplified Model

The repetitive controller is implemented in the closed loop feedback system of the linear magnetostrictive actuator shown in Fig. 3.11.

This is a dual closed-loop feedback system including a feedback position-control loop and a feedback current-control loop. For the feedback position-control loop, the position of the actuator is measured by the laser distance sensor and directed to the position controller, which is a PID controller in this thesis. For the feedback current-control loop, the output of the current controller is sent to a PWM amplifier to generate a PWM signal

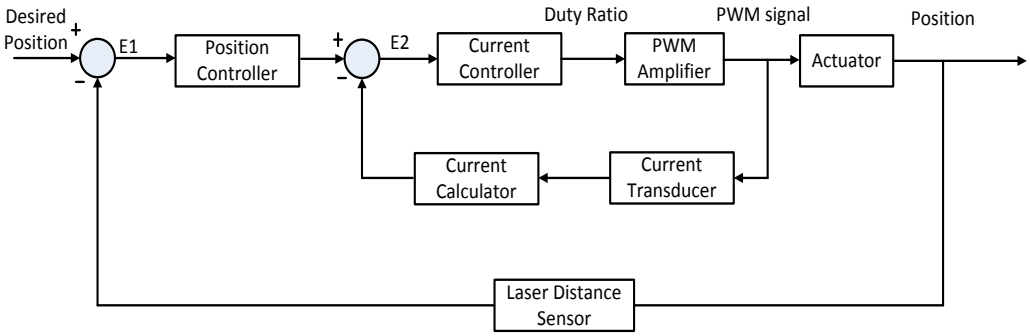

Fig. 3.11. Schematic diagram of the closed loop feedback system [5]

to control the phase current in the magnetostrictive actuator. The real-time current is measured by a current transducer and then calculated by a current calculator to achieve the peak-phase current. Finally it is directed to the current controller.

Normally, the design of the repetitive controller depends on a known plant model. However, this linear magnetostrictive actuator is a nonlinear system with various nonlinearities, such as hysteresis, saturation of the power amplifiers, friction variation, slip during the operation, etc. Since it is difficult to obtain an accurate nonlinear model for the plant with consideration of all these nonlinearities, a simplified plant model is introduced as follows.

It was shown that the speed of this actuator is a function of the peak magnetostrictive strain, external load, and operation frequency [33]. In the linear magnetostrictive actuator with local multiphase excitation, the empirical model is given by (2.1) [1]. From (2.1), if the actuator is operated at a certain frequency with a fixed external load, the speed of the actuator is determined by the phase current.

Consider the open-loop system of the actuator, where the input $X(s)$ is current signal, and the output $Y(s)$ is position signal as indicated in Fig. 3.12.

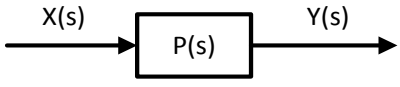

Fig. 3.12. Schematic diagram of the open loop system

Given a step input of the phase current,

$$x(t) = a(t)\ ,\ X(s) = \frac{a}{s} \tag{3.20}$$

and the position output is

$$y(t) = bt\ ,\ Y(s) = \frac{b}{s^2} \tag{3.21}$$

Hence the transfer function is given by

$$P(s) = \frac{Y(s)}{X(s)} = \frac{b}{a} \cdot \frac{1}{s} = \frac{k}{s},\ \text{where}\ \ k = \frac{b}{a} \tag{3.22}$$

which is the simplified model of the actuator.

In the previous research [25], under a 2-A phase current with a 10-Hz excitation frequency, the speed of the actuator was 0.1 mm/s, thus $k = 0.05$ in equation (3.22).

3.3.2 Implementation

A basic model of the RC system is shown in Fig. 3.13, where C_p is the position controller, and C_I is the current controller. The Q filter is not implemented in this control structure and there is no forward loop connected between the error signal and the input of the position controller C_p. In this model, a repetitive controller is added to the existing feedback system, aiming to control the position output by changing the PWM signal.

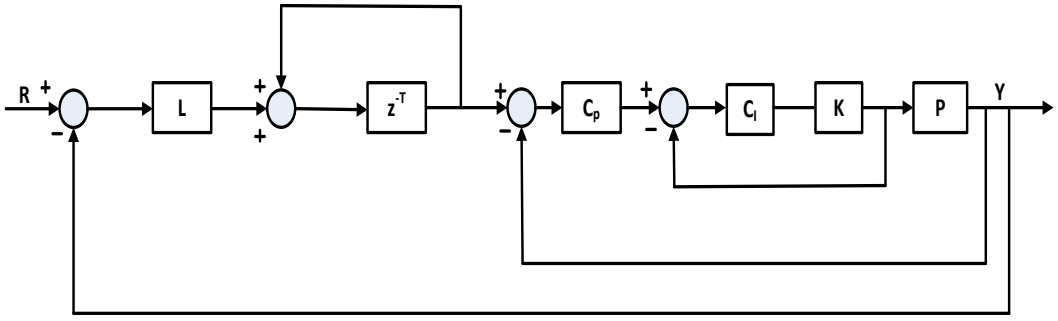

Fig. 3.13. The basic model of the RC system

Here, the transfer function of the learning controller is an inversed closed-loop plant which is given as follows.

$$L(z^{-1}) = G_{CL}{}^{-1}(z^{-1}) \tag{3.23}$$

where

$$G_{CL}(s) = \frac{KC_P(s)C_I(s)P(s)}{1 + KC_I(s)(1 + C_P(s)P(s))} \tag{3.24}$$

$$C_I(s) = \frac{1}{s} \tag{3.25}$$

$$C_p(s) = 40.12 + \frac{40.12}{2.55s} + \frac{25.58s}{0.001s + 1} \tag{3.26}$$

Since the transfer function of the learning controller is an inversed closed loop plant, when applying (3.8), it is easy to notice that the stability condition is met. Simulation results of this design and other designs will be presented in the next chapter.

Note that there is no forward loop connected between the error signal and the input of the position controller in this structure. Therefore, in the first period of the reference

signal, the error information is stored in the delay component and is not sent to the input of the position controller. It indicates that the response of the entire system will be delayed for a period of the reference signal.

As mentioned above, the model is uncertain in high frequencies. In order to resolve this problem, a LPF is introduced as shown in Fig. 3.14. To achieve the best tracking performance, $\left|Q(z^{-1})\right|$ should be as close as 1 at low frequencies. Therefore, a Butterworth filter is selected in the design.

The Butterworth filter has a flat passband. It is regarded as a maximally flat magnitude filter first introduced in 1930 by Butterworth [34].A Butterworth filter has the property that it has a monotonically changing magnitude function with ω for all the orders

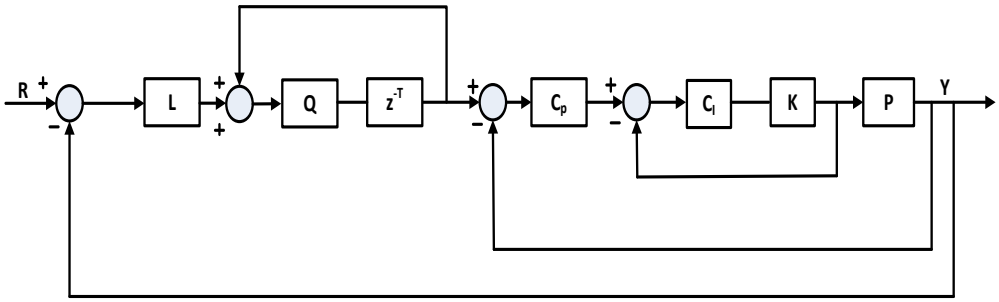

Fig. 3.14. RC closed-loop system with low pass filter Q

of the filter. The only difference of the Butterworth filters with various orders is that the decay rate. For the first-order Butterworth filter, the decay rate is −6 dB per octave (−20 dB per decade). For a second-order filter the decay rate is −12 dB per octave and for a third-order it is −18 dB. A first-order filter can work well to stabilize the system at high frequencies and is chosen in this design.

The cut-off frequency of the filter is selected by 30 rad/s and 60 rad/s to compare the system performance and the robustness. The discrete transfer function of the Butterworth filter is given below with the sampling period of 0.001s.

$$Q\_Butterworth\_low = \frac{0.01478 + 0.01478z^{-1}}{1 - 0.9704z^{-1}} \tag{3.27}$$

$$Q\_Butterworth\_high = \frac{0.02913 + 0.02913z^{-1}}{1 - 0.9417z^{-1}} \tag{3.28}$$

The poles of the filter is located at $z = 0.9417$ which is inside the unit circle. Therefore, this Butterworth filter is stable.

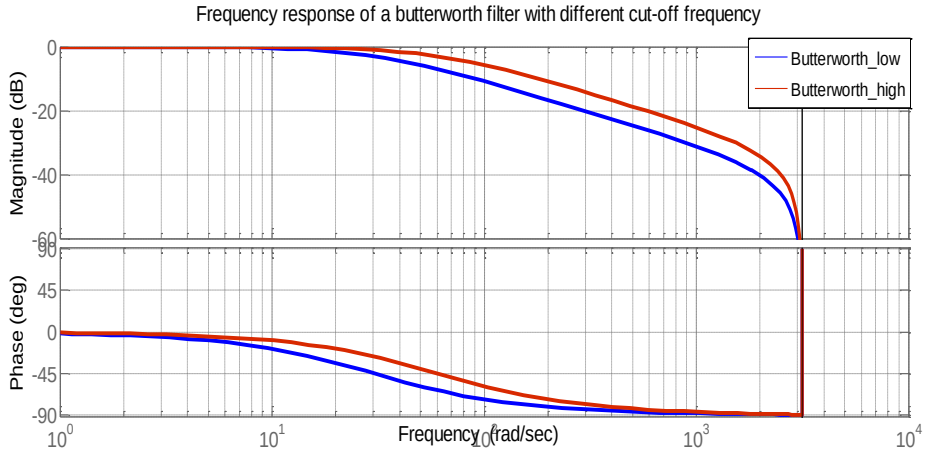

Fig. 3.15. Frequency response of Butterworth filters with different cut-off frequency

As shown in Fig. 3.15, $\left|Q(z^{-1})\right| \approx 1$ at low frequencies, and $\left|Q(z^{-1})\right| < 1$ at frequencies which is higher than the cut-off frequency. An LPF with a higher cut-off frequency provides a wider passband where the system performance is not compromised,

but the stability may not be ensured. Such a trade-off between the robustness and the performance has to be considered when designing the cut-off frequency.

If a quick response is required, a forward loop connected between the error signal and the input of the position controller could be introduced as shown in Fig. 3.16.

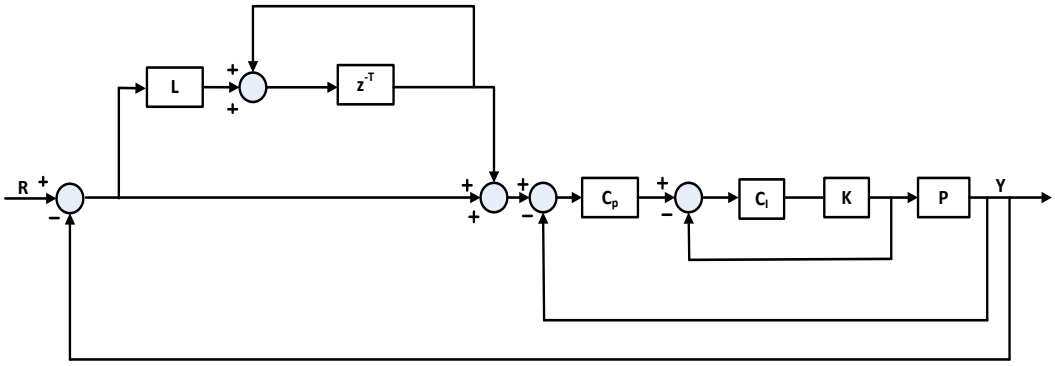

Fig. 3.16. RC closed-loop system with forward loop

CHAPTER IV

SIMULATION AND EXPERIMENTAL RESULTS

In this chapter, the simulation and experimental results is given by implementing the repetitive controller to the novel linear magnetostrictive actuator. The experimental tracking performance of the actuator is also demonstrated.

4.1 Simulation Results

In the simulation, the sampling period of 0.001 s and 0.1 s are applied for comparison. Simulation results with different sampling periods are shown in Figs. 4.1 and 4.2. In fact, the sampling period of 0.001 s is unnecessary in experiments since the bandwidth of the system is very low, the actuator cannot respond to the control signal with the 0.001 s interval.

A sinusoidal signal with a period of 100 s and a magnitude of 1 mm and a triangular wave with a period of 100 s and a magnitude of 1 mm are used as reference signals in simulation. The period of 100 s is selected due to the fact that the bandwidth of the system is very low. Therefore, a reference signal with a large period is applied to ensure the system has enough time to respond to the reference signal.

4.1.1 Basic Structure of RC

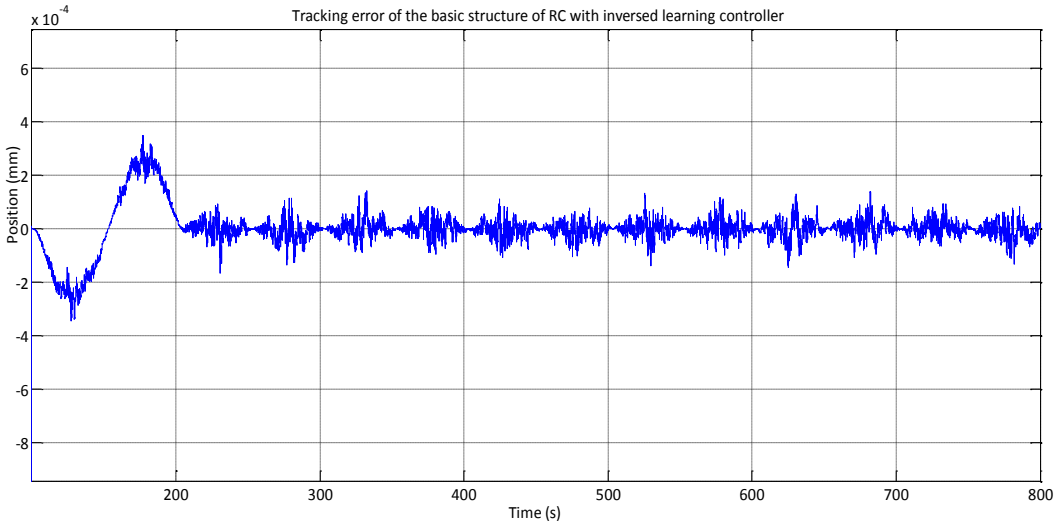

Fig. 4.1. Tracking error of the basic structure of the RC with an inversed controller (sampling period: 0.001 s)

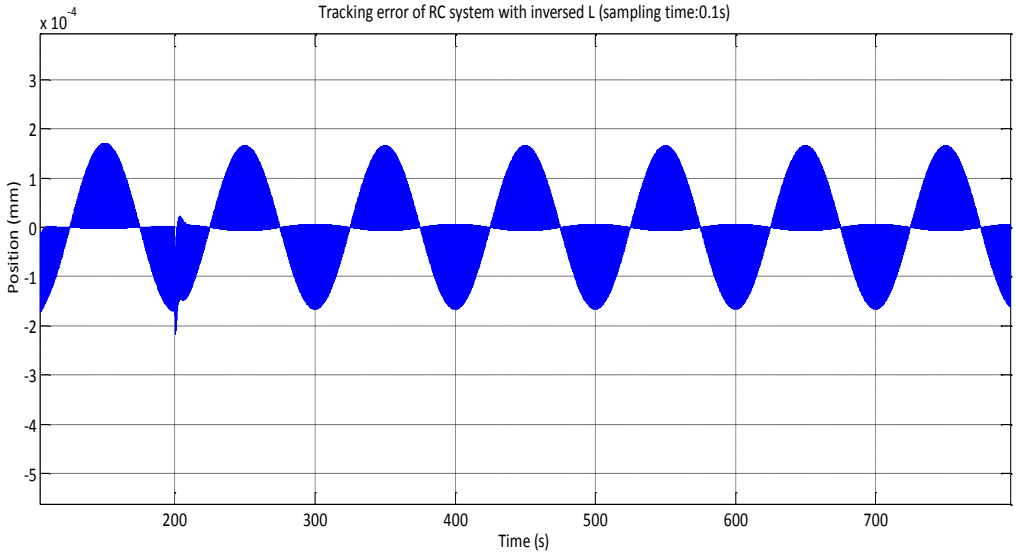

Fig. 4.2. Tracking error of the RC system with an inversed L (sampling period: 0.1 s)

The block diagram of this structure was shown in Fig. 3.13. Compared with the basic structures of the RC system with different sampling periods, the simluation results represent that the tracking error is almost the same, approximately 0.15 μm. It indicates that the sampling period does not affect the tracking perforamce. However, the shape of the error signal is different due to the fact that the sampling period is different. Discrete sampling incidents are expected in the simulation, but the simulation result is shown as a continuous signal by Matlab/Simulink as shown in Fig. 4.3.

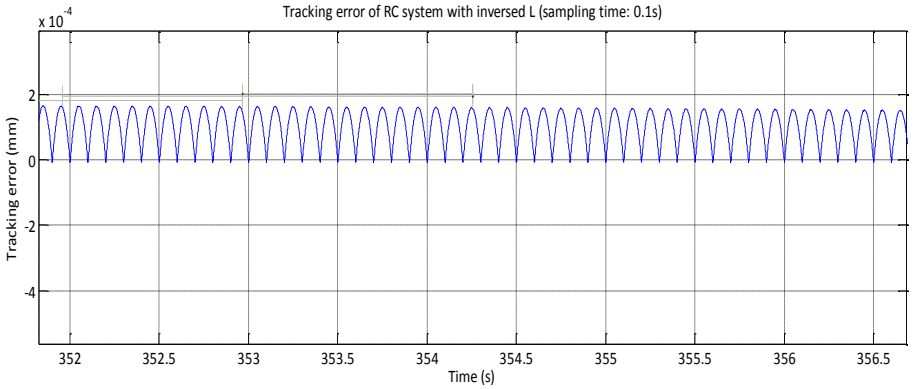

Fig. 4.3. Ripples (sampling period: 0.1 s)

4.1.2 Basic Structure of RC with a Forward Loop

Basic structure of RC with a forward loop is implemented in simulation. The block diagram of this structure was shown in Fig. 3.13. In simulation, the sampling periods of 0.001 s and 0.1 s are applied for comparison. The tracking performances to a sinusoidal input and a triangular wave are presented in Figs. 4.4 – 4.7.

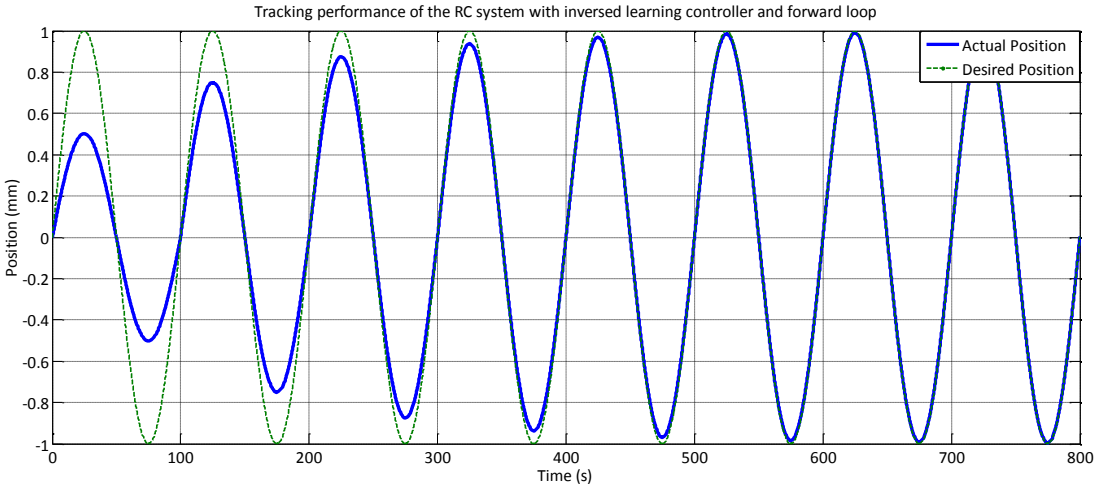

Fig. 4.4. Tracking performance of the RC system with an inversed learning controller and a forward loop (sampling period: 0.001 s)

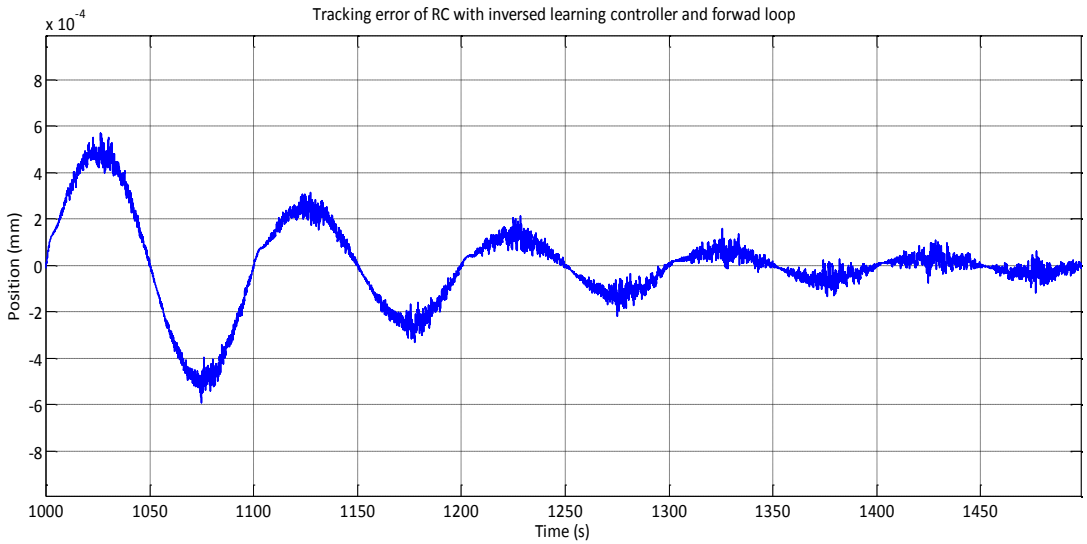

Fig. 4.5. Tracking error of the RC system with an inversed learning controller and a forward loop after 10 periods of the reference signal (sampling period: 0.001 s)

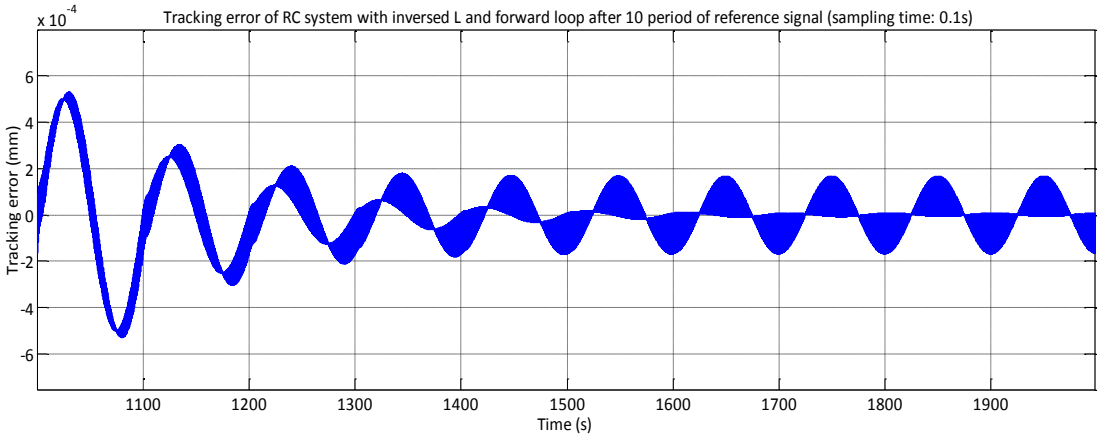

Fig. 4.6. Tracking error of the RC system with an inversed learning controller and a forward loop after 10 periods of the reference signal (sampling period: 0.1 s)

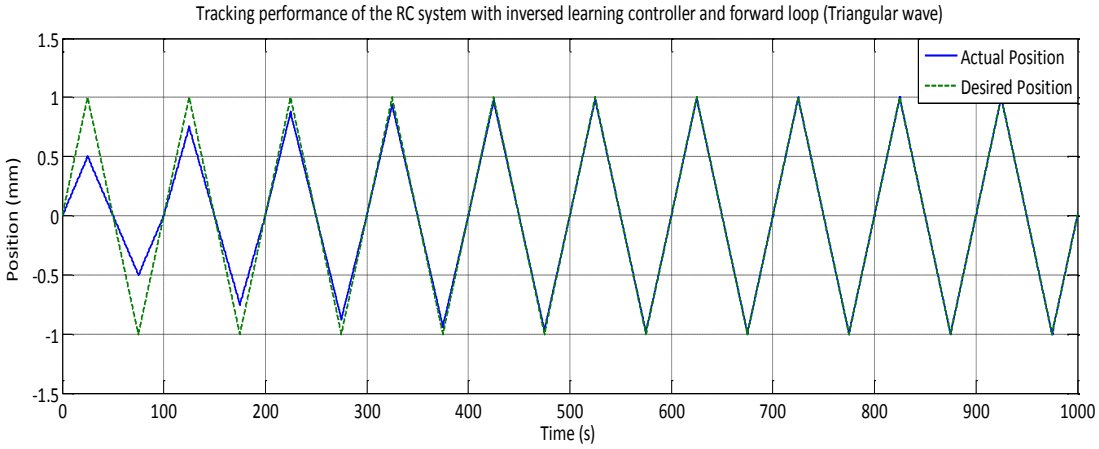

Fig. 4.7. Tracking performance of the RC system to a triangular wave with an inversed learning controller and a forward loop (sampling period: 0.001 s)

As shown in Fig. 4.5 and Fig. 4.6, the response of the basic structure of RC with a forward loop has the following characteristics. First, it has a faster response compared with the one with no forward loop. For the system with no forward loop, the system

response is also delayed by one period of the reference signal since there is a delay of one period of the reference signal in the periodic-signal generator. Second, the convergence rate is slower than that with no forward loop. Comparing the simulation results with a 0.1 s sampling period, it takes 13 periods of the reference signal to get the tracking error under 0.2 μm. However, the system with no forward loop just takes 2 periods of the reference signal to get the tracking error under 0.2 μm.

4.1.3 RC with Low-Pass Filter

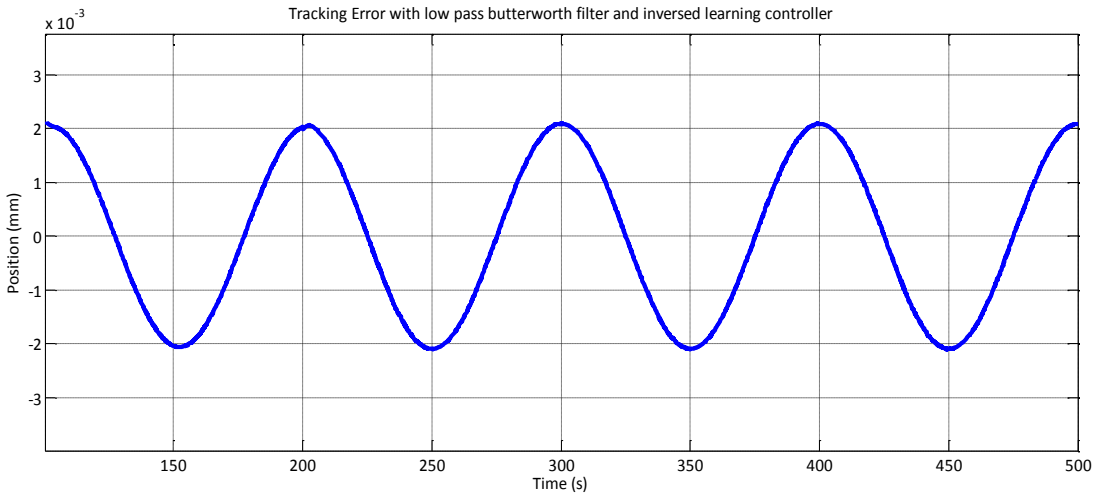

Fig. 4.8. Tracking error with a Butterworth filter with a 30 rad/s cut-off frequency and inversed L (sampling period: 0.001 s)

As shown in Figs. 4.8 and 4.9, the simulation is carried out under a 0.001s sampling period. Comparing the simulation results with different cut-off frequencies, the filter with a higher cut-off frequency has better performance than the one with a lower cut-off

frequency. The tracking errors are 2 μm and 1μm, respectively. It corresponds with the analysis in section 3.2.3. The LPF with a high cut-off frequency can achieve a better tracking performance. However, it may not guarantee the stability of the closed-loop system.

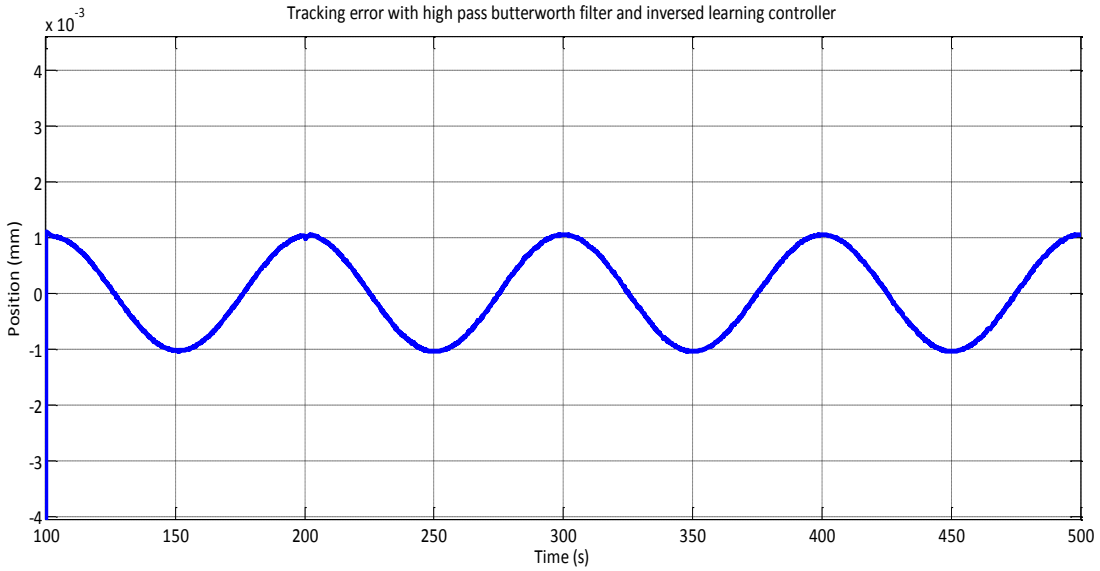

Fig. 4.9. Tracking error with Butterworth filter (60 rad/s cut-off frequency) and inversed L (sampling period: 0.001 s)

Comparing the simulation results between the system with and without a LPF as shown in Fig. 4.1, 4.8, 4.9, it can be seen that the system with no LPF has much better tracking performance with a tracking error of 0.1 μm. On the contrary, the tracking errors with an LPF are 1 μm and 2 μm respectively.

4.2 Experimental Results

Experiments are carried out under the following conditions.

1. Reference input one is $y(t) = 0.5\sin(0.1t) + 18$ in millimeters;

   Reference input two is a triangular wave with a magnitude of 0.5 mm and a period of 100 s.

2. The sampling period is 0.1 s in consideration of the fact that the system has a very low bandwidth.
3. The learning controller is implemented with an inversed closed-loop plant.
4. The LPF Q is not implemented to achieve the best tracking performance.
5. The position controller is a PID controller is tuned by relay auto-tuning method.
6. A forward loop is implemented to achieve a faster system response.

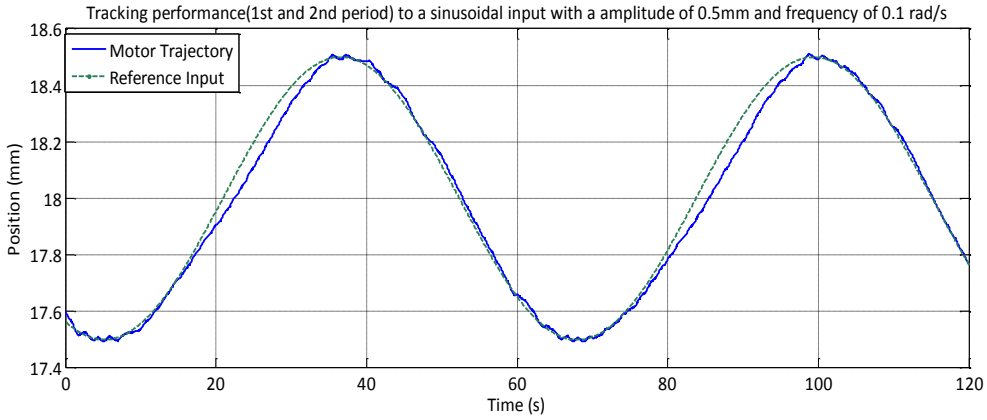

Fig. 4.10. Tracking performance (1st and 2nd periods) to a sinusoidal input with a magnitude of 0.5 mm and frequency of 0.1 rad/s

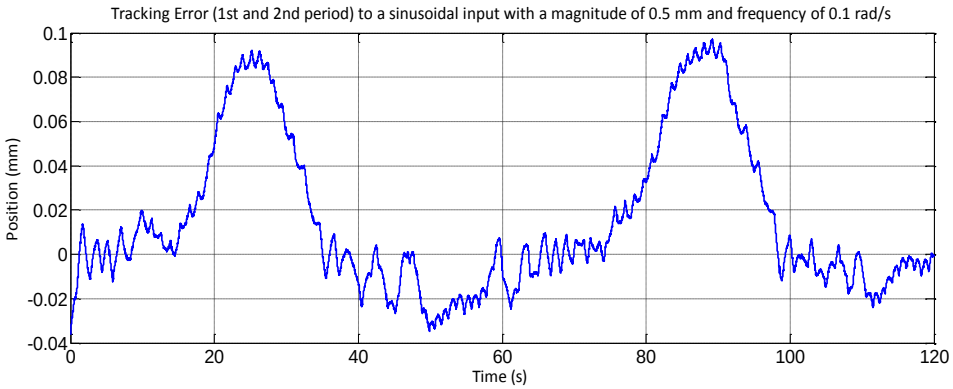

Fig. 4.11. Tracking error (1st and 2nd periods) to a sinusoidal input with a magnitude of 0.5 mm and frequency of 0.1 rad/s

Figs. 4.10 and 4.11 represent the tracking performance and the tracking error to a sinusoidal input with a magnitude of 0.5 mm and frequency of 0.1 rad/s. In most time, the tracking error is under 20 μm. However, when the slope of the reference input is high, which indicates a high velocity is required to track the reference input, the actuator cannot track the reference very well. The reason is that the current is not large enough to move the actuator at such a high speed. The maximum error in such cases is approximately 100 μm.

As shown in Figs. 4.12 and 4.13, the tracking performance enhances after 5 periods of the tracking motion. The maximum error decreases to 30 μm in the 7th period and decreases to approximately 20 μm in the 8th period. The tracking error remains under 20 μm after the 8th period.

Comparing the tracking performance in the 1st period and the 8th period, it seems that the tracking error is minimized by the repetitive controller implemented in the closed-

loop system. However, the PWM signal which controls the phase current is saturated at 1 which means the control effort from the controller is kept the same during the experiment.

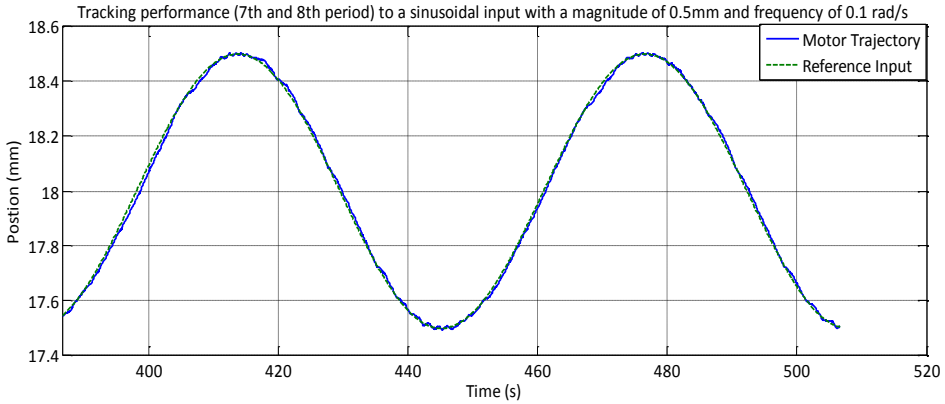

Fig. 4.12. Tracking performance (7th and 8th periods) to a sinusoidal input with a magnitude of 0.5 mm and frequency of 0.1 rad/s

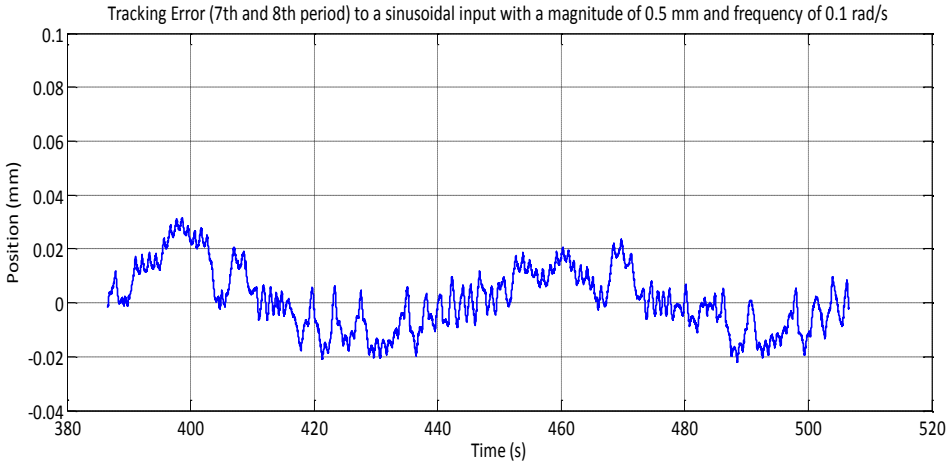

Fig. 4.13. Tracking error (7th and 8th periods) to a sinusoidal input with a magnitude of 0.5 mm and frequency of 0.1 rad/s

Figs. 4.14-4.17 show the tracking performance to a triangular wave input with a magnitude of 0.5 mm and period of 120 s.

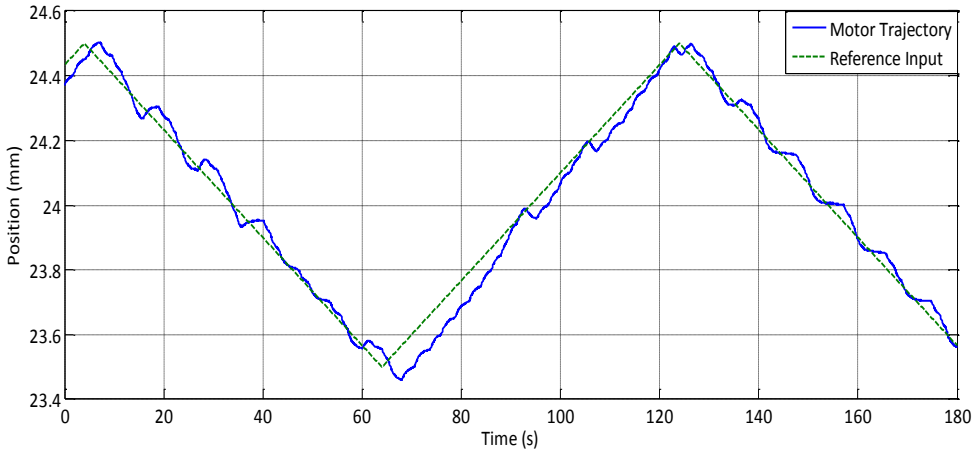

Fig. 4.14. Tracking performance (1st period) to a triangular wave input with a magnitude of 0.5 mm and period of 120 s

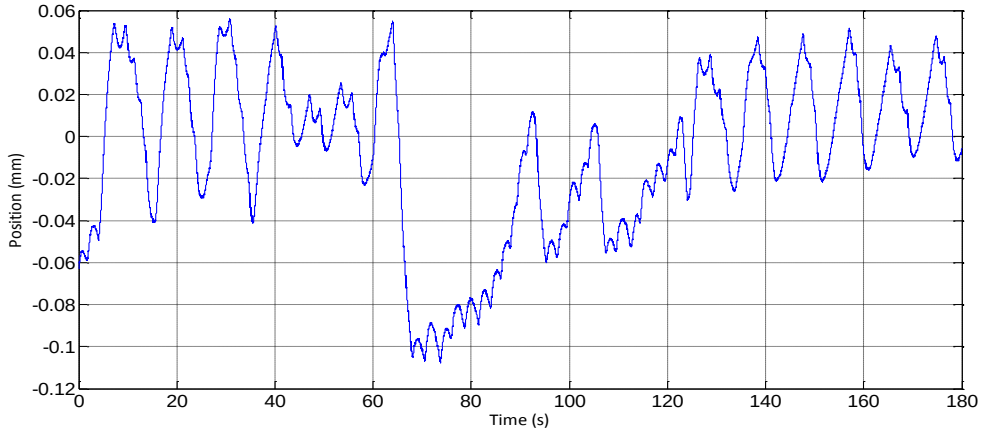

Fig. 4.15.Tracking error (1st period) to a triangular wave input with a magnitude of 0.5 mm and period of 120 s

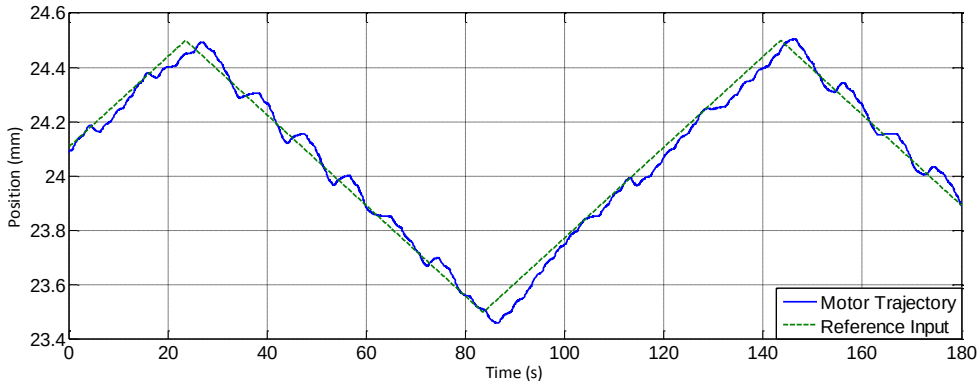

Fig. 4.16. Tracking performance (3th period) to a triangular wave input with a magnitude of 0.5 mm and period of 120 s

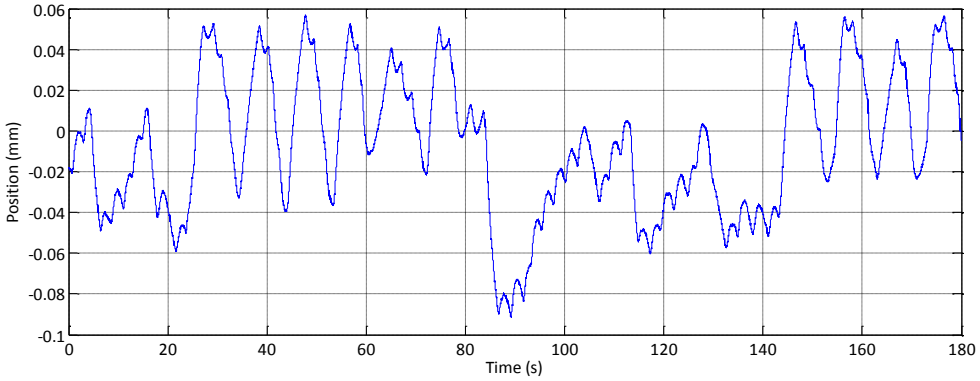

Fig. 4.17. Tracking error (3th period) to a triangular wave input with a magnitude of 0.5 mm and period of 120 s

CHAPTER V

CONCLUSIONS

This chapter summarizes the research and provides suggestions for future work related to RC design in the novel magnetostrictive actuator.

5.1 Conclusions

An RC system was designed after the modification of the previous closed-loop system with position and current controllers. The repetitive controller was designed based on an estimated model of the system. In the repetitive controller, a learning controller was designed to help the actuator track the reference signal precisely. A Butterworth filter was also designed to stabilize the system. Stability, robustness, convergence rate, and performance were discussed in the RC design. The trade-off between robustness and performance was taken into consideration. Both simulation and experiments were carried out in this thesis.

Simulation results showed that the tracking error to a sinusoidal signal with a magnitude of 1 mm could be limited to 0.1 μm. On the other hand, experimental results demonstrated that the tracking error to a sinusoidal reference signal with a magnitude of 0.5 mm and frequency of 0.1 rad/s could decrease to 20 μm after eight periods of tracking contrary to the 100 μm tracking error in the first period.

The comparison with previous research is shown in Fig. 5.1. The selected previous result is the closed-loop response to a sinusoidal reference input with an amplitude of 0.5

mm and frequency of 0.04 rad/s tuned by a relay auto-tuning method [5]. Around $t = 65$ s, the maximum tracking error is over 100 μm which is 20% of the reference signal. Besides, a reverse movement exists in each step of the peristaltic motion.

The maximum tracking error with a repetitive controller could decrease to 20 μm, which is 4% of the reference signal. Furthermore, the motor trajectory with a repetitive controller is much cleaner than that without a repetitive controller. The reverse movement in each step of the peristaltic motion does not exist.

The errors in experiments is much larger than those in simulation. The repetitive controller is designed based on an estimated model, however, this magnetostrictive actuator is a nonlinear system with many nonlinearities such as hysteresis, saturation of the power amplifiers, friction variation, and slip during the operation. These nonlinearities could increase the experimental error.

Note that the laser position sensor has a resolution of 5 μm. It could insert a 10 μm peak-to-peak position noise. This noise may increase the tracking error in the experiments. Besides, the A/D quantization noise and the electrical noise may contribute to this error [5].

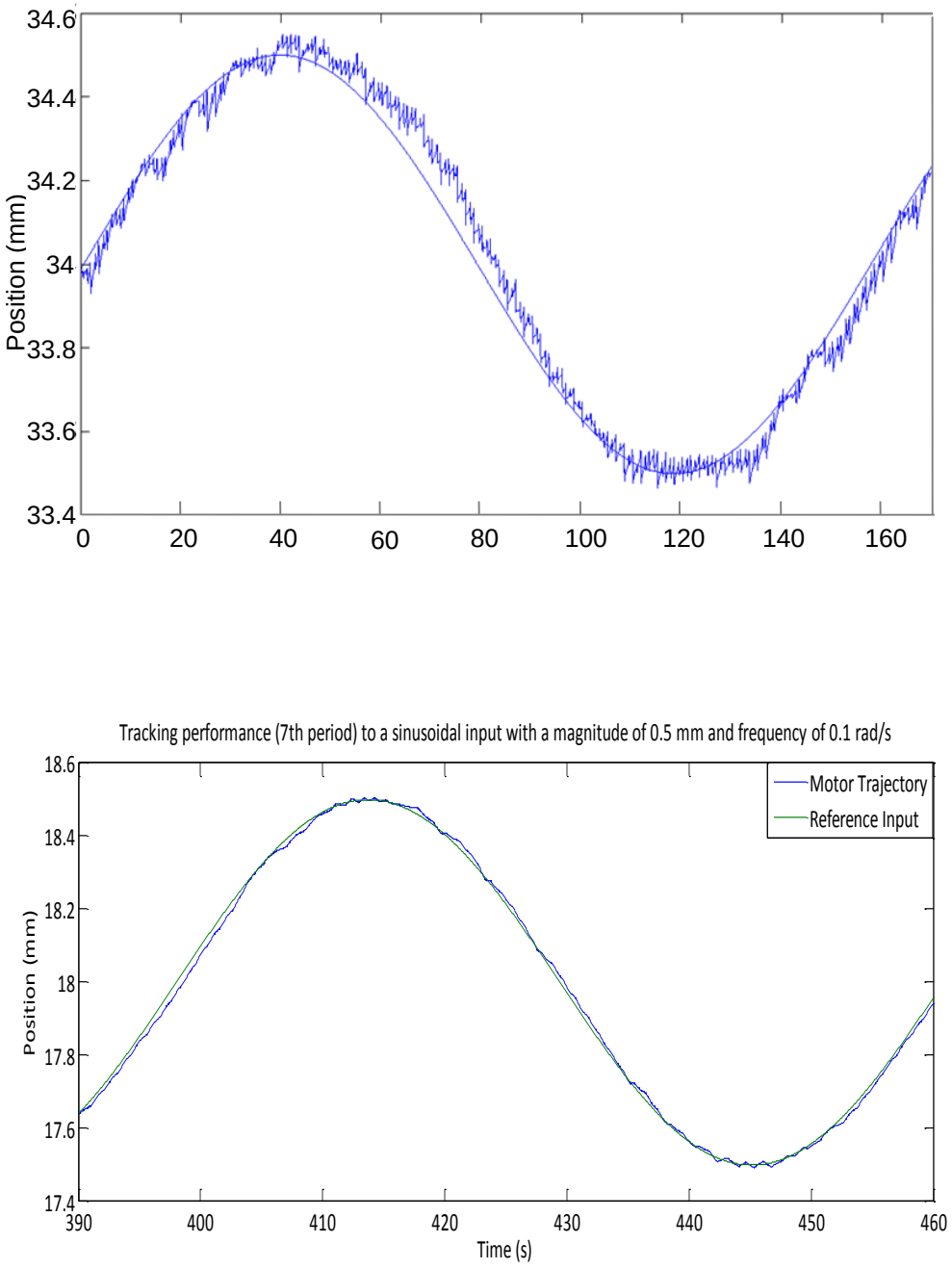

Fig. 5.1. Comparison with previous result

5.2 Suggestions for Future Work

Although the RC system has been successfully implemented in the novel linear magnetostrictive actuator, some aspects of this actuator are still undeveloped. The suggested future work is given as follows.

- The PWM signal was saturated during the experiment with the implementation of the repetitive controller. This may indicate that the maximum power of the PWM amplifier is not enough to execute the control effort. A PWM amplifier with a larger power capacity is suggested to improve the tracking performance.
- The repetitive controller was designed with the consideration of a known and certain periodic reference signal. However, the period of the reference signal could change in practical applications. It is also common that the reference signal has some uncertainties and varies during the operation of the system. A robust RC system could make the controller less sensitive to uncertainties, which is suggested as the future work.
- The resolution of the laser sensor limits the position accuracy of the actuator due to a noise. Sensors with higher resolution are suggested to reduce the noise and enhance the performance.

REFERENCES

[1] Kim W, Sadighi A. A novel low-power linear magnetostrictive actuator with local three-phase excitation [J]. IEEE/ASME Transactions on Mechatronics, April 2010, 15(2): 299–307.

[2] Sadighi A, Kim W. Sensorless control of a novel linear magnetostrictive motor [J]. IEEE Transactions on Industry Applications, May 2011, 47(2): 736–743.

[3] Claeyssen F, Lhermet N, Grosso G. Giant magnetostrictive alloy actuators [J]. International Journal of Applied Electromagnetics in Materials, 1993, 5(1): 67–73.

[4] Claeyssen F, Lhermet N, Le Letty R, Bouchilloux P. Actuators, transducers and motors based on giant magnetostrictive materials [J]. Journal of Alloys and Compounds, August 1997, 258(1): 61–73.

[5] Chen C F. Closed-loop real-time control of a novel linear magnetostrictive actuator [T], Master's Thesis: Texas A&M University, August 2010.

[6] Kiesewetter, "Magnetostrictive Ambler Motor." U.S. Patent 5,281,875, issued January 25, 1994.

[7] Li J H, Gao X X, Xie J X, Zhu J, Bao X Q, Yu R B. Large magnetostriction and structural characteristics of $Fe_{83}Ga_{17}$ wires [J]. Physica B: Condensed Matter, April 2012, 407(8): 1186–1190.

[8] Kim W J, Goldie J H, Gerver M J, Kiley J E, Swenbeck J R. Extended-range linear magnetostrictive motor with double-sided three-phase stators [J]. IEEE Transactions on Industry Applications, May/June 2002, 38(3): 651–659.

[9] Zhang T, Jiang C, Zhang H, Xu H B. Giant magnetostrictive actuators for active vibration control [J]. Smart Materials and Structures, June 2004, 13(3): 473.

[10] Monaco E, Franco F, Lecce L. Experimental and numerical activities on damage detection using magnetostrictive actuators and statistical analysis [J]. Journal of Intelligent Material Systems and Structures, July 2000, 11(7): 567–578.

[11] Monaco E, Franco F, Lecce L. Structural damage identification using magnetostrictive actuators [C]// Symposium on Smart Structures and Materials. International Society for Optics and Photonics, June 1999: 395–404.

[12] Plummer A, Hätönen J, Owens D H. Using repetitive control to eliminate periodic disturbances in damper test rigs [C]// World Congress. 2005, 16(1): 245–245.

[13] Inoue T, Nakano M, Kubo T, Iwai S. High accuracy control of a proton synchrotron magnet power supply [C]// Proceedings of the 8th World Congress of IFAC. 1981, 20: 216–221.

[14] Inoue T, Nakano M, Iwai S. High accuracy control of servomechanism for repeated contouring [C]// 10th Annual Symp. on Incremental Motion Control Systems and Devices. 1981: 285–292.

[15] Francis B A, Wonham W M. The internal model principle of control theory [J]. Automatica, September 1976, 12(5): 457–465.

[16] Wang Y, Gao F, Doyle III F J. Survey on iterative learning control, repetitive control, and run-to-run control [J]. Journal of Process Control, December 2009, 19(10): 1589–1600.

[17] Hara S, Yamamoto Y. Stability of repetitive control systems [C]// 24th IEEE

Conference on Decision and Control, 1985, 24: 326–327.

[18] Hara S, Omata T, Nakano M. Synthesis of repetitive control systems and its application [C]// 24th IEEE Conference on Decision and Control, 1985, 24: 1387–1392.

[19] Nakano M, Hara S. Microprocessor-based repetitive control [M]// Microprocessor-based control systems. Springer Netherlands, 1986: 279–296.

[20] Tomizuka M, Tsao T C, Chew K K. Discrete-time domain analysis and synthesis of repetitive controllers [C]// Proceedings of 1988 American Control Conference, 1988: 860–866.

[21] Hillerstrom G. Adaptive suppression of vibrations-a repetitive control approach [J]. IEEE Transactions on Control Systems Technology, January 1996, 4(1): 72–78.

[22] Hattori S, Ishida M, Hori T. Suppression control method for torque vibration of brushless dc motor utilizing repetitive control with fourier transform [C]// Proceedings. 6th International Workshop on Advanced Motion Control, 2000: 427–432.

[23] Kempf C, Messner W C, Tomizuka M, Horowitz R. Comparison of four discrete-time repetitive control algorithms [J]. IEEE Control Systems Magazines, December 1993, 13(6): 48–54.

[24] Cosner C, Anwar G, Tomizuka M. Plug in repetitive control for industrial robotic manipulators [C]// Proceedings of IEEE International Conference on Robotics and Automation, 1990: 1970–1975.

[25] Sadighi A, Development of a Novel Linear Magnetostrictive Actuator [D], PhD

Dissertation: Texas A&M University, August 2010.

[26] Alciatore D G and Histand M B, Introduction to mechatronics and measurement systems [M]. 3rd Ed., Mc-Graw Hill, New York, 2007.

[27] MOSFET Characteristics Curve, Electronics Tutorials, [Online]. Available: http://www.electronics-tutorials.ws/transistor/tran_7.html. Accessed January 2014.

[28] Product Description of DS1104 R&D Controller Board by dSPACE Inc., Paderborn, Germany, [Online]. Available: http://www.dspace.com/en/inc/home/products/hw/singbord/ds1104.cfm. Accessed March 2014.

[29] Product Description of Laser Distance Sensor (model OADM 20I6460/S14F) by Baumer Inc., Southington, USA [Online]. Available: http://www.baumer.com. Accessed March 2014.

[30] Tharayil M L. Switched Q-filters in Repetitive Control and Iterative Learning Control [D], PhD Dissertation: University of Illinois at Urbana-Champaign, 2005.

[31] Skogestad S, Postlethwaite I. Multivariable feedback control: analysis and design [M]. 2nd Ed., Wiley, Hoboken, New Jersey, 2005.

[32] Tomizuka M. Zero phase error tracking algorithm for digital control [J]. Journal of Dynamic Systems, Measurement and Control, March 1987, 109(1): 65–68.

[33] Goldie J H, Gerver M J, Kiley J E, Swenbeck J R. Observations and theory of Terfenol-D inchworm motors [C]// Proceedings of 5th Annual International Symposium on Smart Structures and Materials, 1998: 780–785.

[34] Butterworth S. On the theory of filter amplifiers [J]. Wireless Engineer, October 1930, 7: 536–541.

APPENDIX A

MATLAB CODE

```
clear all;

close all;

clc;

ts = 0.001;

T=100;              % period of the reference

D=T/ts;

k=5*10^-2;

P=1.7659;

T_p_s= tf(k,[1 0]);              %Model Plant

T_p_z= c2d(T_p_s,ts);                % Discretization Plant


%PID controller

C_kp_s=40.12;

C_ki_s=tf(40.12,[2.55 0]);

C_kd_s=tf([40.12*0.6375 0],[0.001 1]);

C_pid_s=C_kp_s+C_ki_s+C_kd_s;


% current controller

C_i_s=tf(1.7659,[1 1.7659]);
```

```
%C.L. Plant
T_cl_s=(P*C_pid_s*C_i_s*T_p_s)/(1+P*C_i_s*(1+C_pid_s*T_p_s));
T_cl_z=c2d(T_cl_s,ts);
%Learning filter
T_l_z=tf([1*T_cl_z.den{1,1}],T_cl_z.num{1,1},ts,'Variable','z^-1')
% butterworth Q
w_butter_low=30;
w_butter_high=60;
[Q_butterlow1_num,Q_butterlow1_den]=butter(1,w_butter_low*ts/pi,'low');
[Q_butterlow2_num,Q_butterlow2_den]=butter(2,w_butter_low*ts/pi,'low');
[Q_butterhigh_num,Q_butterhigh_den]=butter(1,w_butter_high*ts/pi,'low');
Q_butterlow1=tf(Q_butterlow1_num,Q_butterlow1_den,ts,'Variable','z^-1');
Q_butterlow2=tf(Q_butterlow2_num,Q_butterlow2_den,ts,'Variable','z^-1');
Q_butterhigh=tf(Q_butterhigh_num,Q_butterhigh_den,ts,'Variable','z^-1');
%L memory loop transfer function
T_m_z_n=[T_l_z.num{1,1}];
T_m_z_d=conv([1 zeros(1,D-1) -1],T_l_z.den{1,1});
T_m_z=tf(T_m_z_n,T_m_z_d,ts);
%with butter Q memory loop transfer function
T_butter_num_low1=conv([zeros(1,D) 1],conv([Q_butterlow1_num],T_l_z.num{1,1}));
T_butter_den_low1=conv(([Q_butterlow1_den                    zeros(1,D)]-[zeros(1,D)
Q_butterlow1_num]),T_l_z.den{1,1});
```

```
T_butter_low1=tf(T_butter_num_low1,T_butter_den_low1,ts,'Variable','z^-1');


T_butter_num_high=conv([zeros(1,D) 1],conv([Q_butterhigh_num],T_l_z.num{1,1}));
T_butter_den_high=conv(([Q_butterhigh_den                    zeros(1,D)]-[zeros(1,D)
Q_butterhigh_num]),T_l_z.den{1,1});
T_butter_high=tf(T_butter_num_high,T_butter_den_high,ts,'Variable','z^-1');
```

APPENDIX B

SIMULATION BLOCK DIAGRAM

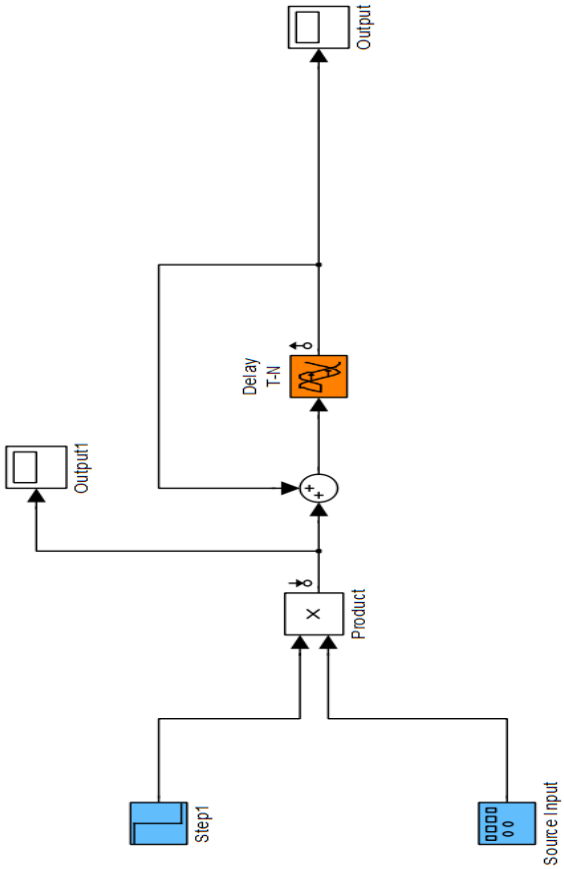

Fig. B.1. Simulink block diagram for periodic signal generator

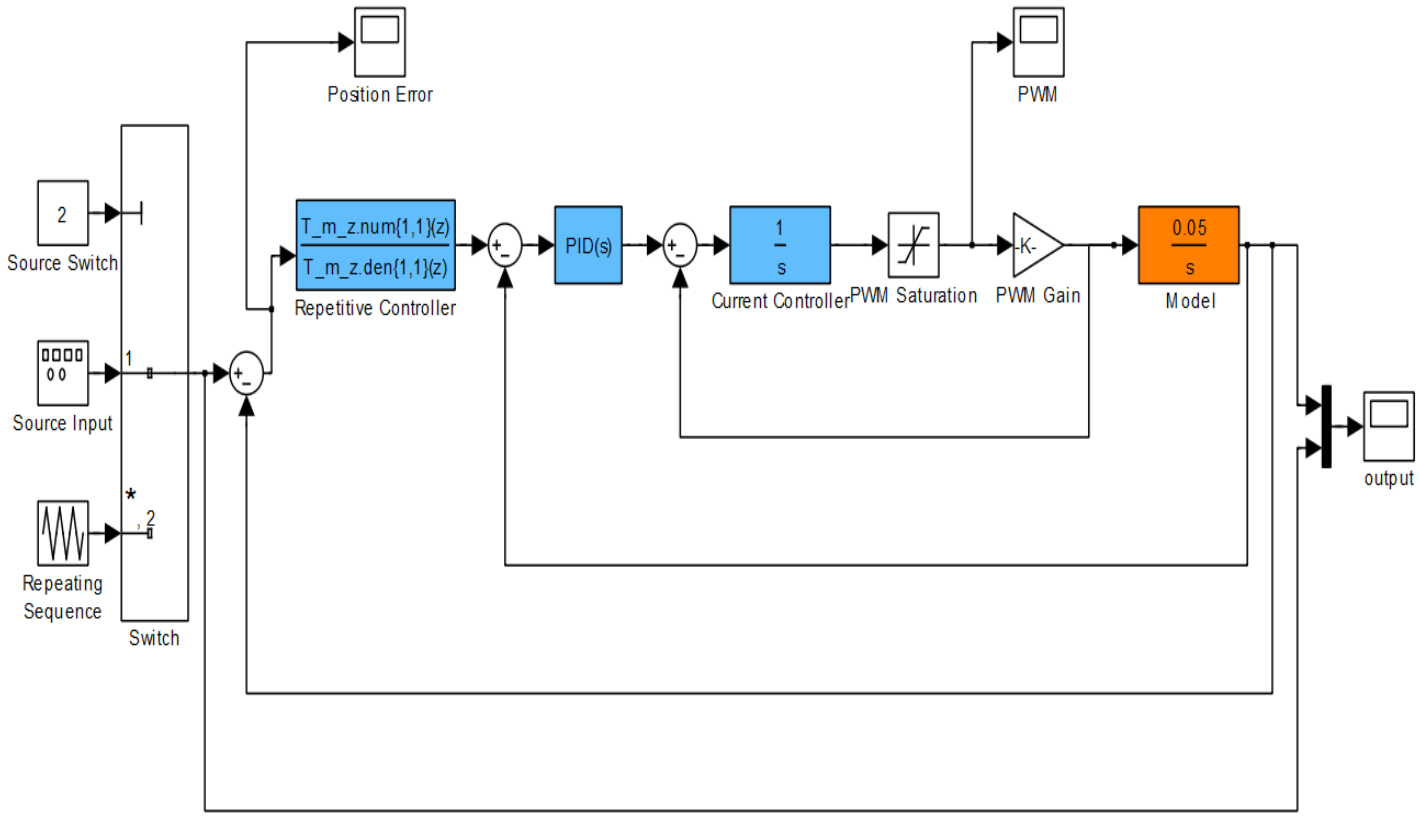

Fig. B.2. Simulink block diagram for repetitive control simulation

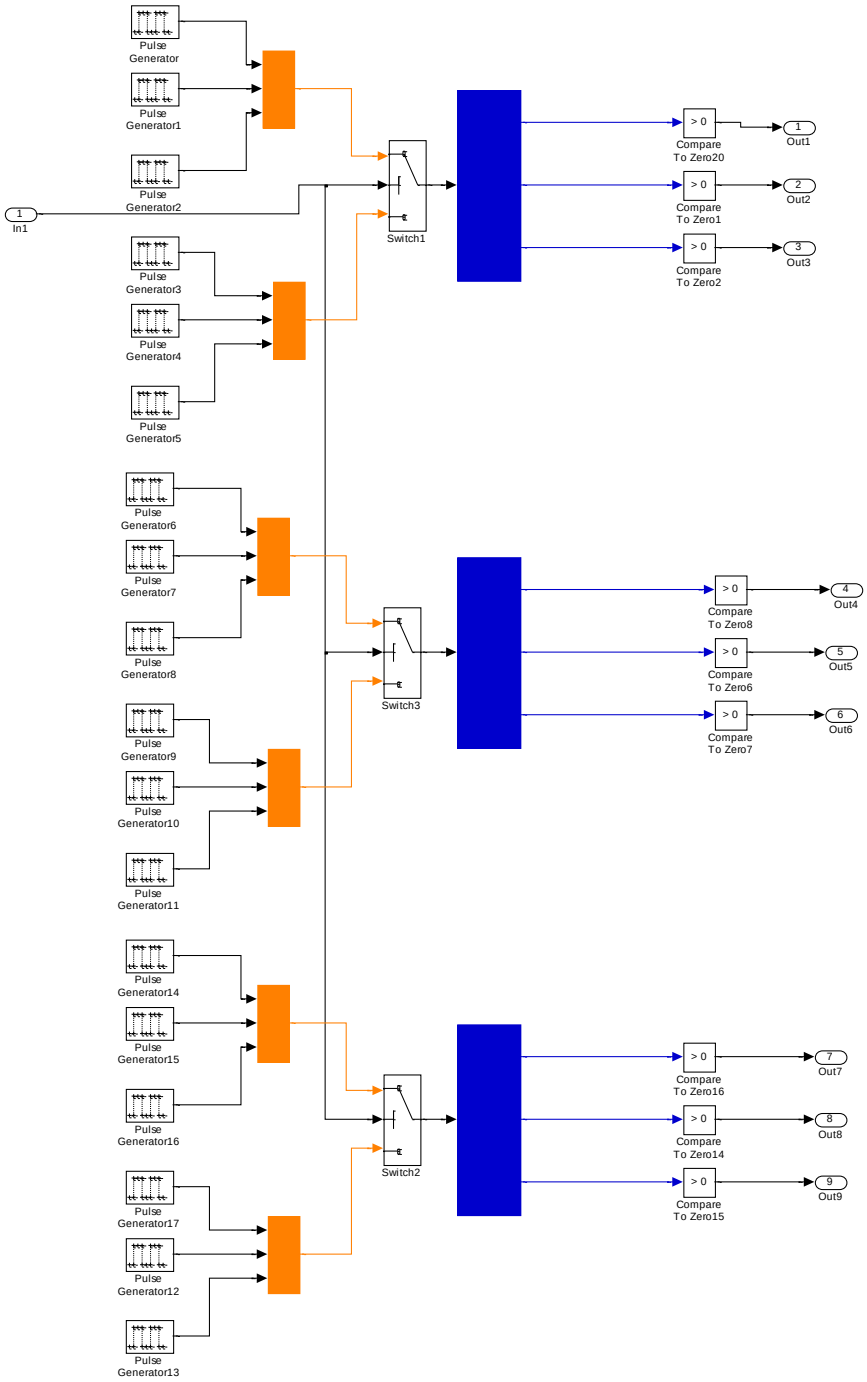

Fig. B.3. Simulink block diagram for switching pulse generator [25].